The Astrophysical Journal, 644:525–542, 2006 June 10

NEARBY DEBRIS DISK SYSTEMS WITH HIGH FRACTIONAL LUMINOSITY RECONSIDERED

A. Moór,[1] P. Ábrahám,[1] A. Derekas,[2,3] Cs. Kiss,[1] L. L. Kiss,[2] D. Apai,[4,5] C. Grady,[6,7] and Th. Henning[8]
Received 2005 December 2; accepted 2006 February 8

ABSTRACT

By searching the *IRAS* and *ISO* databases, we compiled a list of 60 debris disks that exhibit the highest fractional luminosity values ($f_d > 10^{-4}$) in the vicinity of the Sun ($d < 120$ pc). Eleven out of these 60 systems are new discoveries. Special care was taken to exclude bogus disks from the sample. We computed the fractional luminosity values using available *IRAS*, *ISO*, and *Spitzer* data and analyzed the Galactic space velocities of the objects. The results revealed that stars with disks of high fractional luminosity often belong to young stellar kinematic groups, providing an opportunity to obtain improved age estimates for these systems. We found that practically all disks with $f_d > 5 \times 10^{-4}$ are younger than 100 Myr. The distribution of the disks in the fractional luminosity versus age diagram indicates that (1) the number of old systems with high f_d is lower than was claimed before, (2) there exist many relatively young disks of moderate fractional luminosity, and (3) comparing the observations with a current theoretical model of debris disk evolution, a general good agreement could be found.

Subject headings: circumstellar matter — infrared: stars — stars: kinematics

1. INTRODUCTION

One of the major discoveries of the *IRAS* mission was that main-sequence stars may exhibit excess emission at infrared (IR) wavelengths (“Vega phenomenon;” Aumann et al. 1984). Systematic searches in the *IRAS* catalogs (Backman & Paresce 1993; Mannings & Barlow 1998; Silverstone 2000; Zuckerman & Song 2004a and references therein) revealed that ~15% of main-sequence stars show infrared excess (Plets & Vynckier 1999). It was suggested already after the first discovery that the excess can be attributed to thermal emission of dust confined into a circumstellar disk (Aumann et al. 1984). The existence of such *debris disks* was first confirmed by the coronagraphic observation of scattered light from the β Pic system (Smith & Terrile 1984). Subsequent imaging of specific systems at mid-infrared (e.g., HR 4796A; Koerner et al. 1998) and submillimeter wavelengths (e.g., ϵ Eri; Holland et al. 1998) supported this picture.

The possibility that debris disks might evolve over time was first mentioned by Backman & Gillett (1987), who proposed that disks around Vega, ϵ Eridani, and Fomalhaut could be more evolved analogs of the β Pic system. Using submillimeter measurements of the best known Vega-like stars, Holland et al. (1998) showed that the derived dust mass of the disks decays with stellar age as a power law. Subsequent studies with the *Infrared Space Observatory* (*ISO*; Kessler et al. 1996) demonstrated that debris disks are more common around young stars ($t < 400$ Myr) than around old ones and there is a trend for older debris disks to be less massive than younger ones (Habing et al. 2001; Spangler et al. 2001; Silverstone 2000). The evolutionary picture was further refined by Decin et al. (2003), who reinvestigated the *ISO* results and revised the stellar age estimates. Recently Rieke et al. (2005) presented a survey of A-type stars, performed at 24 μm with the Multiband Imaging Photometer for *Spitzer* (MIPS; Rieke et al. 2004) on board the *Spitzer Space Telescope* (Werner et al. 2004), and observed a general decay on a timescale of 150 Myr.

A new generation of theoretical models has been developed to explain the temporal evolution of debris disks (Kenyon & Bromley 2002; Dominik & Decin 2003; Kenyon & Bromley 2004). These models take into account the fact that the destruction timescales of dust grains orbiting main-sequence stars are significantly shorter than the age of the central star; therefore, the observed dust grains in a debris disk must be continuously replenished (Backman & Paresce 1993). Collisional erosion of minor bodies in exosolar analogs of our solar system and the sublimation of comets are the best explanations for the replenishment process (Harper et al. 1984; Backman & Paresce 1993). Most recent models link the temporal evolution of debris disks to the formation and erosion of planetesimals (Kenyon & Bromley 2002, 2004).

The amount of dust in a debris disk is usually characterized by its fractional luminosity, f_d, defined as the ratio of integrated infrared excess of the disk to the bolometric luminosity of the star. Despite the general evolutionary trend described above, fractional luminosity values of individual systems were found to show a large spread of $10^{-6} \lesssim f_d \lesssim 10^{-3}$ at almost any age (Decin et al. 2003). Rieke et al. (2005) also found large variations of the IR excess around A-type stars within each age group. They emphasized the role of individual collisional events between large planetesimals as one of the possible explanations of their result.

Particularly interesting is the relatively high number of older systems ($t \gtrsim 500$ Myr) with high fractional luminosity values ($f_d \simeq 10^{-3}$). These systems pose a serious challenge even to the new generation of theoretical models. A qualitative explanation for the existence of debris disks with large f_d values around old stars was suggested by Dominik & Decin (2003). According to their theory, different planetesimal disks become active debris systems at different ages because of the delayed onset of collisional cascades.

[1] Konkoly Observatory of the Hungarian Academy of Sciences, P.O. Box 67, H-1525 Budapest, Hungary.
[2] School of Physics A28, University of Sydney, Sydney NSW 2006, Australia.
[3] School of Physics, Department of Astrophysics and Optics, University of New South Wales, Sydney NSW 2052, Australia.
[4] Steward Observatory, University of Arizona, 933 North Cherry Avenue, Tucson, AZ 85721.
[5] NASA Astrobiology Institute.
[6] Eureka Scientific, 2452 Delmer Street Suite 100, Oakland, CA 94602-3017.
[7] Exo-Planets and Stellar Astrophysics Laboratory, Exploration of the Universe Division, NASA Goddard Space Flight Center, Code 667, Greenbelt, MD 20771.
[8] Max-Planck-Institut für Astronomie, Königstuhl 17, D-69117 Heidelberg, Germany.

The presence of relatively old systems with high fractional luminosity, however, might partly be an observational artifact, since several factors could bias the distribution of debris disks on the f_d versus age diagram. Some stars have been nominated as Vega candidates due to erroneous infrared photometric measurements, confusion by background sources, or the presence of extended nebulosity (where the IR emission is of interstellar rather than of circumstellar origin). In order to obtain a reliable picture of debris disk evolution, these misidentifications ("bogus disks") have to be found and discarded. The actual positions of confirmed debris disks in the f_d versus age diagram might also be biased by measurement errors in the far-infrared photometry and even more significantly uncertainties in the age determination.

In this paper we study a sample of debris disks that exhibit the highest fractional luminosity values in the solar neighborhood. Setting a threshold value of $f_d = 10^{-4}$ and a distance limit of 120 pc, we compiled a list of 60 disks and performed an accurate determination of their infrared excess using *IRAS*, *ISO*, and *Spitzer* data (§ 2). In § 3 we present improved age estimates for a large number of stars, derived, e.g., by determining their membership in young moving groups. In § 4 we analyze the distribution of the disks in the f_d versus age diagram and find a significant fraction of our sample to be younger than was previously thought.

Our conclusions are summarized in § 5. In Appendix A we list bogus disks identified in our work. Appendix B lists new members of young moving groups discovered in the present study.

2. SAMPLE SELECTION

We created the input list for this study by (1) identifying debris disk candidates in the *IRAS* and *ISO* databases, (2) rejecting bogus debris disks and suspicious objects, and (3) computing infrared fractional luminosity values and selecting disks with $f_d > 10^{-4}$.

2.1. *Searching the IRAS Catalogs for Stars with Infrared Excess*

With the aim of compiling a list of main-sequence stars with IR excess, we made a systematic search in the *IRAS* Faint Source Survey Catalog (FSC; Moshir et al. 1989) and in the *IRAS* Serendipitous Survey Catalog (SSC; Kleinmann et al. 1986). In order to reduce source confusion, our survey was confined to $|b| \geq 10°$ Galactic latitudes. We selected all infrared sources with at least moderate flux quality at 25 or 60 μm, and their positions were correlated with entries from the *Hipparcos* Catalogue (ESA 1997) and the Tycho-2 Spectral Type Catalogue (Wright et al. 2003). Positional coincidences within 30″ were extracted. In order to assure that the selected objects are not giant stars, the luminosity class was constrained to IV–V in the *Hipparcos* catalog and to V in the Tycho catalog. We also included several objects whose luminosity class was not available in the *Hipparcos* catalog but whose absolute magnitudes indicated a main-sequence evolutionary phase. Since the infrared excess from early B-type stars might be due to free-free emission (Zuckerman 2001), the sample was limited to spectral types later than B9 in both catalogs. Our query is similar to that of Silverstone (2000), but since we also considered the *IRAS* 25 μm band, it is also sensitive to stars with excess from warmer dust disk.

Following the principles of the method by Plets & Vynckier (1999), for each selected star we predicted the far-infrared flux density of the stellar photosphere using the K_s-band magnitude (or V band, when good quality K_s photometry was not available) and the $B - V$ color index. K_s-band photometry was drawn from the Two Micron All Sky Survey (2MASS) catalog (Cutri et al. 2003), and V magnitudes and $B - V$ color indices were taken from the *Hipparcos* and Tycho catalogs. As a first step a photospheric 25 μm flux density was derived from the K_s magnitude and the $B - V$ color of the star using the collection of stellar model predictions by M. Cohen and P. Hammersley (available on the *ISO* Data Centre Web site[9]). Then, color relationships predicting the photospheric flux ratios between 25 μm and a selection of *IRAS*, *ISO*, and *Spitzer* photometric bands were also derived from the same stellar models. The average accuracy of the predicted far-infrared fluxes is estimated to be around 4% when computed from the K_s magnitudes and 8% when computed from V magnitudes.

In order to compute IR excess values, the predicted photospheric flux densities were subtracted from the measured flux densities in each *IRAS* band. In principle the *IRAS* fluxes have to be color corrected since the shape of the spectral energy distribution of the system usually differs from the $F_\nu \sim \nu^{-1}$ reference spectrum (this spectral shape was assumed while the flux densities quoted in the *IRAS* catalogs were derived from the detector in-band powers). Since the true spectrum of the system is not known a priori, we decided to multiply the predicted photospheric fluxes (rather than dividing the *IRAS* flux densities) with color correction factors appropriate for a stellar photosphere (Beichman et al. 1988). The significance level of the infrared excess was calculated in each photometric band with the following formula:

$$S_{\rm excess} = \frac{F_{\rm meas} - F_{\rm pred}}{\sqrt{\delta F^2_{\rm meas} + \delta F^2_{\rm pred}}}, \tag{1}$$

where $\delta F_{\rm meas}$ is the quoted uncertainty in the FSC or SSC and $\delta F_{\rm pred}$ is the uncertainty of the prediction described above. When $S_{\rm excess}$ was greater than 3 either in the 25 or 60 μm bands, the object was selected as an excess candidate star. Applying the above criteria, we identified in total 355 excess candidate stars in the *IRAS* databases.

2.2. *ISO-based Selection of Stars with Infrared Excesses*

In a second step the *IRAS*-based list was supplemented with excess stars selected from the *ISO* databases. The Vega phenomenon was a key program for *ISO* (see § 1), and a number of stars have been observed with ISOPHOT, the onboard photometer (Lemke et al. 1996). We collected all ISOPHOT observations of normal stars from different observers performed in minimap, sparse map, or staring mode (a detailed description of these observing modes is given in Laureijs et al. 2003) and performed a homogeneous reevaluation of the whole sample (Ábrahám et al. 2003; P. Ábrahám et al. 2006, in preparation). For details of the data analysis and criteria for candidate excess stars, see P. Ábrahám et al. (2006, in preparation). We note that most selected candidates have already been published by the original observers (Decin et al. 2000; Habing et al. 2001; Spangler et al. 2001; Silverstone 2000), but due to their different processing schemes, the published flux densities cannot be directly merged for a homogeneous catalog. The merged *IRAS*- and *ISO*-based list includes altogether 364 IR excess stars.

2.3. *Rejection of Suspicious Objects*

Since our goal is to compile a list of debris disks, we excluded all known young stellar objects (e.g., T Tauri or Herbig Ae/Be stars) that harbor protoplanetary disks. The sample could also be contaminated by source confusion: due to the low spatial

[9] Available at http://www.iso.vilspa.esa.es/users/expl_lib/ISO/wwwcal.

resolution of *IRAS* at far-IR wavelengths, many of the positional coincidences between a star and a far-IR source could be bogus and the far-IR emission is related to a foreground or background object.

For part of the sample (110 stars) higher spatial resolution infrared maps are available, obtained by either the ISOPHOT or MIPS instrument. We downloaded ISOPHOT data from the *ISO* Data Archive (IDA) and processed with the Phot Interactive Analysis (PIA) version 10.0 (Gabriel et al. 1997). MIPS basic calibrated data (BCD) files were downloaded from the *Spitzer* Science Center data archive. The latter products are composed of two-dimensional FITS image files that included all general calibrations and corrections for MIPS detectors (Gordon et al. 2005). In each case these data were co-added and corrected for array distortions with the *Spitzer* Science Center MOPEX (MOsaicking and Point source EXtraction; Makovoz & Marleau 2005) software. Bad data flagged in the BCD mask files, as well as permanently damaged pixels flagged in the static pixel mask file, were ignored during the data combination. Output mosaics had pixels with size of 2.″5 at 24 μm and 4″ at 70 μm. The MOPEX/APEX software package was used to detect sources and determine their positions on the final maps.

The positions of the infrared sources were determined on the *ISO* and *Spitzer* maps, and objects whose coordinates differed from the optical position (and in some cases coincided with a nearby background object) and/or associated with extended nebulosity were discarded from the list. For positional discrepancy the threshold value was set to half of the width of a point source's footprint. In the case of ISOPHOT the large pixel size dominated the footprint, and in the 60–100 μm range the threshold was 23″. In the case of MIPS arrays the footprint was defined by the telescope point-spread function, and we adopted threshold values of 3″ and 9″ at 24 and 70 μm, respectively. The absolute pointing uncertainty was less than these values for both satellites. In total 24 disk candidates were dropped from the list.

When neither *ISO* nor *Spitzer* maps were available, we made an attempt to filter out bogus disks by assuming that an object is possibly affected by source confusion if one of the following applies:

1. A known galaxy or evolved star (OH/IR source, Mira variable) is located within 1′ of the *IRAS* position.
2. A source included in the *IRAS* Small Scale Structure Catalog (Helou & Walker 1988) or in the 2MASS Extended Source Catalog (Jarrett et al. 2000) is located within 1′ of the *IRAS* position.
3. A 2MASS source with an excess in the K_s band (identified in the $H - K_s$ vs. $J - H$ diagram in comparison with the locus of the main sequence and taking into account the reddening path) is located within 1′ of the *IRAS* position.
4. The 60 μm/100 μm flux ratio of the candidate source resembles the color of infrared cirrus ($F_{60}/F_{100} < 0.25$, which corresponds to blackbody temperatures lower than 33 K). At least moderate flux quality flags were required in both *IRAS* bands.

These cases were also discarded from our list of debris disk candidates (48 objects).

In an earlier study, Kalas et al. (2002) used high angular resolution coronagraphic observations at optical wavelengths and found cases where the far-infrared excess observed by *IRAS* was of interstellar (rather than circumstellar) origin ("Pleiades phenomenon"), leading to false entries in the Vega candidate lists. They also suggested that a significant fraction of Vega candidates beyond the Local Bubble might be bogus, since the star illuminates nearby interstellar matter rather than a circumstellar disk. After checking the positions of our sources projected on recent maps of the Local Bubble (Lallement et al. 2003), we discarded all objects situated in the wall of the bubble or beyond. The wall was defined as the isocontours corresponding to the 50 mÅ Na I D2 line equivalent widths in the maps. In practice nearly all of our sources beyond 120 pc were removed, while within this radius only a few were dropped. Thus, we defined a maximum distance limit of 120 pc for our stars, constructing a nearly complete volume-limited sample.

2.4. *The List of Disks with High Fractional Luminosity*

In order to compute fractional luminosity values for each candidate star, we constructed spectral energy distributions by combining infrared fluxes from the FSC, SSC, and ISOPHOT (reevaluated by us; see P. Ábrahám et al. 2006, in preparation) and additional MIPS and submillimeter fluxes from the literature. The excess above the predicted photosphere was fitted by a single-temperature modified blackbody, where the emissivity was assumed to vary as $1 - \exp\left[-(\lambda_0/\lambda)^{\beta}\right]$, where λ_0 was set to 100 μm (see, e.g., Williams et al. 2004). We fixed β equal to 1, which is a typical value in the case of debris systems (Dent et al. 2000). If the excess was detected at one wavelength only, we adopted a modified blackbody whose peak (in F_ν) coincided with that single wavelength. From the fitted spectral shape color correction factors were computed and applied to the data. Then again a modified blackbody was fitted, resulting in new color correction factors, and this procedure was repeated until the color correction factors converged. Finally, the fractional dust luminosity was calculated as $f_d = L_{\rm IR}/L_{\rm bol}$. In order to estimate the uncertainties on our fractional luminosity values, we performed a Monte Carlo simulation. We added Gaussian noise to the photometric data points using their quoted 1 σ photometric errors and then recomputed the fractional dust luminosities. Formal uncertainties of the predicted theoretical photospheric fluxes were also taken into account. Final uncertainties were derived as the standard deviation of these values after 1000 repetitions. We note that these values include only random uncertainties; systematic errors due to, e.g., limited wavelength coverage are not taken into account.

Artymowicz (1996) argued that debris disks are confined to $f_d < 10^{-2}$ and sources with higher fractional luminosity probably contain a significant amount of gas (e.g., T Tauri and Herbig Ae/Be stars, "transition" objects). Therefore, we excluded objects with $f_d > 10^{-2}$ from our sample. Then the remaining sample was sorted by decreasing f_d values and stars with $f_d > 10^{-4}$ (60 stars) were taken for the further analysis presented in this paper.

Basic stellar parameters for these 60 objects, as well as derived fractional luminosities and their uncertainties, are presented in Table 1. Infrared data used in our analysis, including both the original flux values as listed in the catalogs or provided by our reduction algorithm and corrected fluxes, where color correction was applied, are given in Table 2. The table also contains photospheric flux predictions for the specific wavelengths. Inspecting the flux density values obtained by different instruments at the same wavelength (e.g., *IRAS* and ISOPHOT at 60 μm), one finds discrepancies that may arise, e.g., from the different beams and different calibration strategies of the instruments. Comparing the *IRAS* and ISOPHOT flux values in Table 2, a general good agreement within 1 σ was found, with no deviations above the 3 σ limit (the uncertainty σ was computed as the quadratic sum of quoted uncertainties from the two instruments). We also compared our ISOPHOT flux densities with the results of earlier evaluations of the same observations in the literature. In most cases the results were consistent (except HD 10647 and HD 53143, where

TABLE 1

Stellar Properties and Derived Fractional Luminosities of the Disks

Name (1)	Other Name (2)	Spectral Type (3)	V (mag) (4)	$B-V$ (mag) (5)	Distance (pc) (6)	First Reference to Debris Disk (7)	Debris Disk Confirmation (8)	References (9)	f_d (10^{-4}) (10)	Age (Myr) (11)	Age References (12)
HD 105	...	G0 V	7.51	0.595	40	1	ISO/MIPS	1, 2	2.5 ± 0.3	30^{+10}_{-20}	30
HD 377	...	G2 V	7.59	0.626	40	2	MIPS	2	4.0 ± 0.3	[30, 100]	31, 32
HD 3003	...	A0 V	5.07	0.038	46	3	MIPS*		1.4 ± 0.2	30^{+10}_{-20}	30
HD 6798	...	A3 V	5.60	0.008	83	4	IRS	12	1.6 ± 0.3	340^{+60}_{-80}	7
HD 8907	...	F8	6.66	0.505	34	1	ISO/MIPS	1, 2	2.4 ± 0.1	[100, 870]	31, 33, 34
HD 9672	49 Cet	A1 V	5.62	0.066	61	5	ISO	13	9.2 ± 0.6	[8, 20]	34, 35
HD 10472	...	F2 IV/V	7.62	0.420	67	1	MIPS*	14	3.4 ± 0.9	[20, 150]	30
HD 10647	...	F8 V	5.52	0.551	17	6	ISO/MIPS*	15	3.0 ± 0.3	[300, 7000]	34, 36
HD 10638	...	A3	6.73	0.247	72	1	...		3.9 ± 0.5	[20, 150]	30
HD 15115	...	F2	6.79	0.399	45	1	ISO/MIPS	1	4.9 ± 0.4	12^{+8}_{-4}	30
HD 15745	...	F0	7.47	0.360	64	1	ISO/MIPS	1	20.1 ± 1.4	<700	34, 36
HD 16743	...	F0/F2 III/IV	6.78	0.387	60	7	MIPS		3.6 ± 0.3	1200^{+500}_{-600}	36
HD 17390	...	F3 IV/V	6.48	0.387	45	1	ISO/MIPS*	16	1.9 ± 0.2	<800	34, 36
HD 21997	...	A3 IV/V	6.38	0.120	74	4	IRS	12	4.7 ± 0.3	20^{+10}_{-10}	30
HD 24966	...	A0 V	6.89	0.023	104	1	...		2.4 ± 0.5	<100	7
HD 25457	...	F5 V	5.38	0.516	19	1	ISO/MIPS	1, 2	1.0 ± 0.2	[50, 100]	30
HD 30447	...	F3 V	7.85	0.393	78	1	ISO/MIPS	16	7.5 ± 1.1	20^{+10}_{-10}	30
HD 32297	...	A0	8.13	0.199	112	1	COR	17	33.4 ± 6.0	<30	37
HD 35841	...	F5 V	8.91	0.496	104[P]	1	...		15.5 ± 3.7	20^{+10}_{-10}	30
HD 37484	...	F3 V	7.26	0.404	60	4	ISO/MIPS	1, 2	2.7 ± 0.5	30^{+10}_{-20}	30
HD 38207	...	F2 V	8.47	0.391	103[P]	1	ISO/MIPS	1, 2	10.8 ± 0.6	20^{+10}_{-10}	30
HD 38206	...	A0 V	5.73	−0.014	69	8	MIPS	18	1.4 ± 0.3	20^{+10}_{-10}	30
HD 38678	ζ Lep	A2 Vann	3.55	0.104	22	9	ISO/MIPS*	19	1.1 ± 0.2	200^{+100}_{-100}	30
HD 39060	β Pic	A3 V	3.85	0.171	19	10	ISO/COR/SUBM	10, 20, 21	24.3 ± 1.1	12^{+8}_{-4}	30
HD 50571	...	F7 III–IV	6.11	0.457	33	7	MIPS*		1.1 ± 0.3	1800^{+1000}_{-1300}	36
HD 53143	...	K0 IV–V	6.81	0.786	18	8	ISO	15	2.0 ± 0.5	980^{+520}_{-330}	15
HD 54341	...	A0 V	6.52	−0.008	93	7	...		1.8 ± 0.4	<100	7
HD 69830	...	K0 V	5.95	0.754	13	8	IRS	22	2.0[a]	[600, 4700]	3, 33
HD 76582	...	F0 IV	5.68	0.209	49	1	...		1.7 ± 0.2	450^{+150}_{-290}	7
HD 78702	...	A0/A1 V	5.73	0.000	80	1	...		2.1 ± 0.7	220^{+100}_{-140}	7
HD 84870A	...	A3	7.20	0.233	90	1	...		4.5 ± 1.0	<520	7
HD 85672	...	A0	7.59	0.159	93	1	...		4.9 ± 1.0	<100	7
HD 92945	...	K1 V	7.72	0.873	22	1	MIPS	23	5.3 ± 1.2	100	32, 33
HD 107146	...	G2 V	7.04	0.604	29	1	MIPS/COR/SUBM	2, 24, 25	9.2 ± 0.9	100^{+100}_{-20}	25, 34
HD 109573A	HR 4796A	A0 V	5.78	0.003	67	11	MIR/COR	26, 27	47.0 ± 2.5	8^{+7}_{-3}	30
HD 110058	...	A0 V	7.99	0.148	100	8	ISO	16	18.9 ± 3.3	<100	7
HD 115116	...	A7 V	7.07	0.205	85	7	...		3.2 ± 1.0	<360	7
HD 120534	...	A5 V	7.02	0.275	67[P]	1	...		4.9 ± 0.9	<320	7
HD 121812	...	K0	8.53	0.820	38	7	...		14.9 ± 4.1	230^{+150}_{-90}	7
HD 122106	...	F8 V	6.36	0.486	78	7	...		1.2 ± 0.4	[1000, 1600]	36, 38
HD 127821	...	F4 IV	6.10	0.428	32	1	MIPS*		2.2 ± 0.4	[200, 3400]	34, 36
HD 130693	...	G6 V	8.20	0.734	33[P]	7	...		5.8 ± 1.9	50^{+50}_{-40}	7
HD 131835	...	A2 IV	7.88	0.192	111	7	...		19.9 ± 3.3	17^{+1}_{-1}	30
HD 157728	...	F0 IV	5.70	0.229	43	6	...		2.9 ± 0.4	<200	7
HD 158352	...	A8 V	5.41	0.237	63	9	...		1.8 ± 0.5	750^{+150}_{-150}	7
HD 164249	...	F5 V	7.01	0.458	47	1	ISO/MIPS*	1	10.4 ± 1.6	12^{+8}_{-4}	30

TABLE 1—*Continued*

Name (1)	Other Name (2)	Spectral Type (3)	V (mag) (4)	$B-V$ (mag) (5)	Distance (pc) (6)	First Reference to Debris Disk (7)	Debris Disk Confirmation (8)	References (9)	f_d (10^{-4}) (10)	Age (Myr) (11)	Age References (12)
HD 169666	. . .	F5	6.68	0.444	51	7	MIPS		1.5 ± 0.3	2200^{+400}_{-600}	36
HD 170773	. . .	F5 V	6.22	0.429	36	5	ISO/MIPS*	1	3.8 ± 0.4	[200, 2800]	34, 36
HD 172555	. . .	A7 V	4.78	0.199	29	9	MIPS*		7.8 ± 0.7	12^{+8}_{-4}	30
HD 181296	η Tel	A0 Vn	5.03	0.020	48	8	ISO/MIPS*	1	2.4 ± 0.2	12^{+8}_{-4}	30
HD 181327	. . .	F5/F6 V	7.04	0.480	51	8	ISO/MIPS*	16	29.3 ± 1.6	12^{+8}_{-4}	30
HD 182681	. . .	B8/B9 V	5.66	−0.014	69	7	. . .		1.5 ± 0.3	<100	7
HD 191089	. . .	F5 V	7.18	0.480	54	8	ISO/MIPS*	16	19.1 ± 2.2	12^{+8}_{-4}	30
HD 192758	. . .	F0 V	7.02	0.317	62[P]	1	ISO/MIPS	16	5.6 ± 0.5	[35, 55]	30
HD 197481	AU Mic	M1 Ve	8.81	1.470	10	1	MIPS/COR/SUBM	23, 28, 29	4.0 ± 0.3	12^{+8}_{-4}	30
HD 202917	. . .	G5 V	8.65	0.690	46	1	MIPS*	1	2.9 ± 0.8	30^{+10}_{-20}	30
HD 205674	. . .	F3/F5 IV	7.19	0.396	53	7	MIPS*		3.5 ± 0.8	2600^{+900}_{-1400}	36
HD 206893	. . .	F5 V	6.69	0.439	39	1	ISO/MIPS*	1	2.3 ± 0.2	<2800	34, 36
HD 218396	. . .	A5 V	5.97	0.259	40	1	ISO	1	2.3 ± 0.2	[20, 150]	30
HD 221853	. . .	F0	7.35	0.405	71	1	ISO/MIPS	1	8.0 ± 1.1	[20, 150]	30

Notes.—Col. (1): Names. Col. (2): Other names. Cols. (3)–(5): Data are from the *Hipparcos* or the Tycho-2 Spectral Type Catalog. Col. (6): Distances. P indicates photometric distances; otherwise, *Hipparcos* distances were used. Col. (7): Reference for first identification as debris disks. Col. (8): Observations following the original *IRAS* discovery that independently confirmed the existence of the debris disk. COR: coronagraphic observation; ISO: ISOPHOT; MIR: observation at mid-infrared wavelengths; IRS: *Spitzer* IRS; MIPS: *Spitzer* MIPS; SUBM: observation at submillimeter wavelengths. An asterisk marks those MIPS observations when we extracted only astrometrical information from the maps but did not determine photometric fluxes. Col. (9): References for papers related to observations of col. (8). Col. (10): Fractional dust luminosities and their uncertainties. Col. (11): Ages estimates; [t1, t2] marks an age interval. Col. (12): References for age estimates.

[a] Beichman et al. (2005b) demonstrated the presence of strong spectral features for this object; therefore, we took their fractional luminosity estimate rather than fitting the photometric points by a modified blackbody.

References.—(1) Silverstone 2000; (2) http://data.spitzer.caltech.edu/popular/feps/20051123_enhanced_v1, FEPS Data Explanatory Supplement v3.0, Hines et al. 2005; (3) Song et al. 2000; (4) Patten & Willson 1991; (5) Sadakane & Nishida 1986; (6) Stencel & Backman 1991; (7) this paper; (8) Mannings & Barlow 1998; (9) Oudmaijer et al. 1992; (10) Smith & Terrile 1984; (11) Jura 1991; (12) Jura et al. 2004; (13) Walker & Heinrichsen 2000; (14) Rebull et al. 2004; (15) Decin et al. 2000; (16) P. Ábrahám et al. 2006, in preparation; (17) Schneider et al. 2005; (18) Rieke et al. 2005; (19) Habing et al. 2001; (20) Heinrichsen et al. 1999; (21) Holland et al. 1998; (22) Beichman et al. 2005b; (23) Chen et al. 2005b; (24) Ardila et al. 2004; (25) Williams et al. 2004; (26) Koerner et al. 1998; (27) Schneider et al. 1999; (28) Krist et al. 2005; (29) Liu et al. 2004; (30) ages of stellar kinematic groups as presented in Table 4; (31) Carpenter et al. 2005; (32) Song et al. 2004; (33) Wright et al. 2004; (34) Zuckerman & Song 2004a; (35) Thi et al. 2001; (36) Nordström et al. 2004; (37) Kalas 2005; (38) Rocha-Pinto et al. 2004.

TABLE 2
SUMMARY TABLE OF FLUXES MEASURED IN EXCESS

Name (1)	Instrument (2)	Wavelength (3)	Measured Flux: Uncorrected (4)	Measured Flux: Corrected (5)	Flux Quality (6)	Photospheric Flux (7)	References (8)
HD 105	ISOPHOT	60	0.107 ± 0.014	0.108 ± 0.014	...	3.9E−03	1
	MIPS	70	0.145 ± 0.012	0.164 ± 0.014	...	2.9E−03	2
	ISOPHOT	90	0.147 ± 0.010	0.159 ± 0.011	...	1.7E−03	1
	MIPS	160	0.166 ± 0.028	0.171 ± 0.029	...	5.5E−04	2
HD 377	MIPS	24	0.035 ± 0.002	0.035 ± 0.002	...	0.025	2
	IRAS	60	0.179 ± 0.014	0.185 ± 0.015	3	4.0E−03	3
	MIPS	70	0.146 ± 0.017	0.158 ± 0.018	...	2.9E−03	2
HD 3003	*IRAS*	25	0.343 ± 0.027	0.320 ± 0.026	3	0.063	4
HD 6798	*IRAS*	25	0.111 ± 0.018	0.108 ± 0.017	3	0.039	4
	IRAS	60	0.403 ± 0.048	0.414 ± 0.050	2	6.7E−03	4
HD 8907	*IRAS*	60	0.285 ± 0.054	0.305 ± 0.058	3	7.4E−03	4
	ISOPHOT	60	0.224 ± 0.020	0.232 ± 0.021	...	7.4E−03	1
	MIPS	70	0.232 ± 0.007	0.256 ± 0.008	...	5.4E−03	2
	ISOPHOT	90	0.264 ± 0.018	0.270 ± 0.018	...	3.3E−03	1
HD 9672	*IRAS*	25	0.384 ± 0.042	0.438 ± 0.048	3	0.041	4
	IRAS	60	2.02 ± 0.12	2.09 ± 0.13	3	7.0E−03	4
	IRAS	100	1.88 ± 0.21	1.85 ± 0.20	2	2.5E−03	4
	ISOPHOT	120	1.45 ± 0.38	1.32 ± 0.35	...	1.7E−03	1
	ISOPHOT	170	0.862 ± 0.181	0.772 ± 0.162	...	8.7E−04	1
HD 10472	*IRAS*	60	0.140 ± 0.032	0.145 ± 0.033	2	2.4E−03	4
HD 10647	*IRAS*	60	0.815 ± 0.106	0.877 ± 0.114	3	0.024	4
	ISOPHOT	60	0.803 ± 0.040	0.824 ± 0.041	...	0.024	1
	IRAS	100	1.08 ± 0.17	1.08 ± 0.17	2	8.7E−03	4
HD 10638	*IRAS*	60	0.348 ± 0.038	0.360 ± 0.040	3	3.6E−03	4
HD 15115	MIPS	24	0.055 ± 0.006	0.054 ± 0.006	...	0.032	5
	IRAS	60	0.441 ± 0.048	0.473 ± 0.052	3	5.1E−03	4
	ISOPHOT	60	0.401 ± 0.019	0.415 ± 0.020	...	5.1E−03	1
	ISOPHOT	90	0.419 ± 0.029	0.427 ± 0.030	...	2.2E−03	1
HD 15745	MIPS	24	0.162 ± 0.016	0.168 ± 0.017	...	0.016	5
	IRAS	25	0.177 ± 0.028	0.207 ± 0.033	2	0.015	4
	IRAS	60	0.868 ± 0.061	0.875 ± 0.061	3	2.6E−03	4
	ISO	60	0.753 ± 0.038	0.770 ± 0.039	...	2.6E−03	1
	ISO	90	0.532 ± 0.037	0.515 ± 0.036	...	1.1E−03	1
HD 16743	MIPS	24	0.049 ± 0.005	0.049 ± 0.005	...	0.029	5
	IRAS	60	0.304 ± 0.033	0.323 ± 0.036	3	4.6E−03	4
HD 17390	*IRAS*	60	0.226 ± 0.034	0.240 ± 0.036	3	6.4E−03	4
	ISO	60	0.253 ± 0.021	0.262 ± 0.022	...	6.4E−03	1
	ISO	90	0.228 ± 0.023	0.231 ± 0.023	...	2.8E−03	1
HD 21997	*IRAS*	60	0.595 ± 0.036	0.646 ± 0.039	3	3.9E−03	4
	IRAS	100	0.636 ± 0.108	0.629 ± 0.107	2	1.4E−03	4
HD 24966	*IRAS*	60	0.184 ± 0.031	0.190 ± 0.032	3	1.9E−03	4
HD 25457	MIPS	24	0.202 ± 0.011	0.204 ± 0.011	...	0.147	2
	IRAS	60	0.287 ± 0.075	0.285 ± 0.074	2	0.023	4
	ISOPHOT	60	0.293 ± 0.030	0.297 ± 0.030	...	0.023	1
	MIPS	70	0.288 ± 0.012	0.310 ± 0.013	...	0.017	2
	ISOPHOT	90	0.246 ± 0.018	0.242 ± 0.018	...	0.010	1
HD 30447	MIPS	24	0.028 ± 0.003	0.028 ± 0.003	...	0.012	5
	IRAS	60	0.274 ± 0.030	0.296 ± 0.033	3	1.9E−03	4
	ISO	60	0.247 ± 0.062	0.256 ± 0.064	...	1.9E−03	1
	ISO	90	0.271 ± 0.065	0.277 ± 0.067	...	8.3E−04	1
HD 32297	*IRAS*	25	0.211 ± 0.034	0.256 ± 0.041	2	5.7E−03	4
	IRAS	60	1.12 ± 0.07	1.14 ± 0.07	3	9.7E−04	4
HD 35841	*IRAS*	60	0.188 ± 0.040	0.195 ± 0.041	...	8.1E−04	4
HD 37484	MIPS	24	0.053 ± 0.003	0.055 ± 0.003	...	0.021	2
	IRAS	60	0.128 ± 0.036	0.124 ± 0.035	2	3.3E−03	4
	ISOPHOT	60	0.094 ± 0.012	0.095 ± 0.012	...	3.3E−03	1
	MIPS	70	0.104 ± 0.011	0.110 ± 0.012	...	2.4E−03	2
	ISOPHOT	90	0.047 ± 0.012	0.044 ± 0.011	...	1.5E−03	1
HD 38207	MIPS	24	0.017 ± 0.003	0.017 ± 0.003	...	6.9E−03	2
	ISOPHOT	60	0.205 ± 0.015	0.212 ± 0.015	...	1.1E−03	1
	MIPS	70	0.178 ± 0.006	0.194 ± 0.007	...	7.9E−04	2
	ISOPHOT	90	0.177 ± 0.013	0.177 ± 0.013	...	4.8E−04	1
HD 38206	MIPS	24	0.115 ± 0.023	0.119 ± 0.024	...	0.033	6
	IRAS	25	0.110 ± 0.021	0.113 ± 0.021	2	0.030	4
	IRAS	60	0.313 ± 0.038	0.313 ± 0.038	3	5.1E−03	4

TABLE 2—*Continued*

Name (1)	Instrument (2)	Wavelength (3)	Measured Flux: Uncorrected (4)	Measured Flux: Corrected (5)	Flux Quality (6)	Photospheric Flux (7)	References (8)
HD 38678	*IRAS*	25	1.16 ± 0.09	0.97 ± 0.08	3	0.296	4
	IRAS	60	0.366 ± 0.073	0.302 ± 0.060	3	0.051	4
	ISOPHOT	60	0.404 ± 0.020	0.390 ± 0.019	. . .	0.051	1
HD 39060	*IRAS*	12	3.40 ± 0.14	2.38 ± 0.10	3	1.09	4
	IRAS	25	8.81 ± 0.35	10.29 ± 0.41	3	0.254	4
	IRAS	60	19.7 ± 0.79	18.92 ± 0.76	3	0.043	4
	IRAS	100	11.0 ± 0.44	9.32 ± 0.37	3	0.015	4
	ISOPHOT	120	7.9 ± 1.2	6.68 ± 1.01	. . .	0.011	1
	ISOPHOT	150	4.80 ± 0.73	4.39 ± 0.67	. . .	6.8E−03	1
	ISOPHOT	170	4.0 ± 0.6	3.29 ± 0.49	. . .	5.4E−03	1
	ISOPHOT	200	2.10 ± 0.35	2.03 ± 0.34	. . .	3.9E−03	1
HD 50571	*IRAS*	60	0.183 ± 0.040	0.186 ± 0.041	2	0.011	4
HD 53143	*IRAS*	60	0.152 ± 0.040	0.155 ± 0.040	2	0.012	4
	ISOPHOT	60	0.214 ± 0.011	0.219 ± 0.011	. . .	0.012	1
	ISOPHOT	90	0.145 ± 0.011	0.142 ± 0.011	. . .	5.1E−03	1
HD 54341	*IRAS*	60	0.203 ± 0.047	0.210 ± 0.048	2	2.7E−03	4
HD 69830	*IRAS*	25	0.341 ± 0.038	0.292 ± 0.032	3	0.142	4
HD 76582	*IRAS*	60	0.391 ± 0.047	0.403 ± 0.048	3	9.2E−03	4
HD 78702	*IRAS*	60	0.314 ± 0.047	0.327 ± 0.049	2	5.6E−03	4
	IRAS	100	0.954 ± 0.267	0.987 ± 0.276	2	2.0E−03	4
HD 84870A...............	*IRAS*	60	0.243 ± 0.046	0.252 ± 0.048	3	2.4E−03	4
HD 85672	*IRAS*	60	0.193 ± 0.037	0.200 ± 0.038	3	1.4E−03	4
HD 92945	*IRAS*	60	0.248 ± 0.045	0.270 ± 0.049	3	6.3E−03	4
	MIPS	70	0.271 ± 0.060	0.301 ± 0.067	. . .	4.6E−03	7
HD 107146	MIPS	24	0.060 ± 0.003	0.059 ± 0.003	. . .	0.042	2
	IRAS	60	0.705 ± 0.056	0.777 ± 0.062	3	6.7E−03	4
	MIPS	70	0.648 ± 0.014	0.727 ± 0.016	. . .	4.9E−03	2
	IRAS	100	0.910 ± 0.155	0.913 ± 0.155	2	2.4E−03	4
	SCUBA	450	0.130 ± 0.040	0.130 ± 0.040	. . .	1.1E−04	8
	SCUBA	850	0.020 ± 0.004	0.020 ± 0.004	. . .	3.2E−05	8
HD 109573A.............	*IRAS*	12	0.284 ± 0.011	0.214 ± 0.009	3	0.131	3
	IRAS	25	3.73 ± 0.00[a]	4.38 ± 0.00[a]	3	0.031	3
	IRAS	60	8.07 ± 0.00[a]	7.71 ± 0.00[a]	3	5.2E−03	3
	IRAS	100	4.09 ± 0.08	3.86 ± 0.08	3	1.9E−03	3
	SCUBA	850	0.019 ± 0.004	0.019 ± 0.004	. . .	2.5E−05	9
HD 110058................	*IRAS*	25	0.266 ± 0.029	0.300 ± 0.033	3	5.7E−03	4
	IRAS	60	0.368 ± 0.062	0.341 ± 0.058	2	9.8E−04	4
	ISOPHOT	60	0.387 ± 0.085	0.387 ± 0.085	. . .	9.8E−04	1
	ISOPHOT	90	0.218 ± 0.050	0.201 ± 0.046	. . .	4.3E−04	1
HD 115116................	*IRAS*	60	0.192 ± 0.054	0.198 ± 0.056	2	2.5E−03	4
HD 120534	*IRAS*	60	0.315 ± 0.047	0.326 ± 0.049	. . .	3.3E−03	4
HD 121812	*IRAS*	60	0.263 ± 0.047	0.289 ± 0.052	3	2.7E−03	4
	IRAS	100	0.484 ± 0.135	0.492 ± 0.138	2	9.6E−04	4
HD 122106	*IRAS*	60	0.161 ± 0.042	0.164 ± 0.043	2	9.2E−03	4
HD 127821	*IRAS*	60	0.344 ± 0.041	0.376 ± 0.045	3	0.011	4
	IRAS	100	0.525 ± 0.137	0.529 ± 0.138	2	3.8E−03	4
HD 130693	*IRAS*	60	0.149 ± 0.042	0.154 ± 0.043	. . .	3.2E−03	4
HD 131835	*IRAS*	25	0.186 ± 0.034	0.224 ± 0.040	2	6.1E−03	4
	IRAS	60	0.684 ± 0.062	0.681 ± 0.061	3	1.0E−03	4
HD 157728	*IRAS*	25	0.213 ± 0.019	0.221 ± 0.020	3	0.053	4
	IRAS	60	0.536 ± 0.048	0.531 ± 0.048	3	9.0E−03	4
HD 158352	*IRAS*	25	0.258 ± 0.044	0.255 ± 0.043	3	0.075	4
	IRAS	60	0.366 ± 0.062	0.348 ± 0.059	2	0.013	4
HD 164249	*IRAS*	60	0.647 ± 0.091	0.669 ± 0.094	2	4.7E−03	4
	ISOPHOT	60	0.740 ± 0.037	0.761 ± 0.038	. . .	4.7E−03	1
	ISOPHOT	90	0.568 ± 0.040	0.560 ± 0.039	. . .	2.1E−03	1
HD 169666	MIPS	24	0.087 ± 0.009	0.090 ± 0.009	. . .	0.039	5
	IRAS	25	0.101 ± 0.013	0.088 ± 0.011	3	0.036	4
HD 170773	*IRAS*	60	0.504 ± 0.086	0.555 ± 0.094	2	9.1E−03	4
	ISOPHOT	60	0.547 ± 0.027	0.562 ± 0.028	. . .	9.1E−03	1
	ISOPHOT	90	0.771 ± 0.054	0.821 ± 0.057	. . .	4.0E−03	1
HD 172555	*IRAS*	12	1.52 ± 0.06	1.34 ± 0.05	3	0.508	4
	IRAS	25	1.09 ± 0.06	0.91 ± 0.05	3	0.119	4
	IRAS	60	0.306 ± 0.046	0.241 ± 0.036	3	0.020	4

TABLE 2—*Continued*

Name (1)	Instrument (2)	Wavelength (3)	Measured Flux: Uncorrected (4)	Measured Flux: Corrected (5)	Flux Quality (6)	Photospheric Flux (7)	References (8)
HD 181296	*IRAS*	12	0.481 ± 0.024	0.351 ± 0.018	3	0.264	4
	IRAS	25	0.491 ± 0.025	0.496 ± 0.025	3	0.061	4
	IRAS	60	0.495 ± 0.045	0.449 ± 0.040	3	0.011	4
	ISOPHOT	60	0.436 ± 0.022	0.433 ± 0.022	...	0.011	1
	ISOPHOT	90	0.307 ± 0.022	0.286 ± 0.021	...	4.6E−03	1
HD 181327	*IRAS*	25	0.248 ± 0.020	0.286 ± 0.023	3	0.027	4
	IRAS	60	1.86 ± 0.07	1.93 ± 0.08	3	4.7E−03	4
	ISOPHOT	60	1.69 ± 0.17	1.73 ± 0.17	...	4.7E−03	1
	ISOPHOT	90	1.40 ± 0.14	1.41 ± 0.14	...	2.1E−03	1
	IRAS	100	1.72 ± 0.21	1.69 ± 0.20	2	1.7E−03	4
	ISOPHOT	170	0.820 ± 0.214	0.736 ± 0.192	...	5.9E−04	1
HD 182681	*IRAS*	60	0.412 ± 0.066	0.426 ± 0.068	2	5.6E−03	4
HD 191089	*IRAS*	25	0.339 ± 0.051	0.387 ± 0.058	2	0.024	4
	IRAS	60	0.711 ± 0.057	0.729 ± 0.058	3	4.1E−03	4
	ISOPHOT	60	0.774 ± 0.080	0.781 ± 0.081	...	4.1E−03	1
	ISOPHOT	90	0.394 ± 0.040	0.370 ± 0.038	...	1.8E−03	1
HD 192758	MIPS	24	0.042 ± 0.004	0.041 ± 0.004	...	0.022	5
	IRAS	60	0.360 ± 0.050	0.388 ± 0.054	...	3.5E−03	4
	ISOPHOT	60	0.370 ± 0.022	0.383 ± 0.023	...	3.5E−03	1
	ISOPHOT	90	0.375 ± 0.026	0.384 ± 0.027	...	1.6E−03	1
HD 197481	*IRAS*	60	0.269 ± 0.046	0.252 ± 0.043	2	0.024	4
	MIPS	70	0.196 ± 0.015	0.207 ± 0.016	...	0.017	7
	SHARC	350	0.072 ± 0.020	0.072 ± 0.020	...	6.8E−04	7
	SCUBA	850	0.014 ± 0.002	0.014 ± 0.002	...	1.1E−04	10
HD 202917	ISOPHOT	60	0.046 ± 0.014	0.047 ± 0.014	...	1.9E−03	1
HD 205674	*IRAS*	60	0.199 ± 0.040	0.205 ± 0.041	3	3.7E−03	4
HD 206893	*IRAS*	60	0.228 ± 0.039	0.247 ± 0.042	3	6.3E−03	4
	ISOPHOT	60	0.234 ± 0.015	0.242 ± 0.016	...	6.3E−03	1
	ISOPHOT	90	0.259 ± 0.018	0.268 ± 0.019	...	2.8E−03	1
HD 218396	*IRAS*	60	0.410 ± 0.061	0.450 ± 0.068	3	8.6E−03	4
	ISOPHOT	60	0.400 ± 0.020	0.412 ± 0.021	...	8.6E−03	1
	ISOPHOT	90	0.553 ± 0.039	0.585 ± 0.041	...	3.8E−03	1
HD 221853	MIPS	24	0.079 ± 0.008	0.082 ± 0.008	...	0.019	5
	IRAS	60	0.327 ± 0.062	0.329 ± 0.062	3	3.0E−03	4
	ISO	60	0.368 ± 0.031	0.376 ± 0.032	...	3.0E−03	1
	ISO	90	0.231 ± 0.016	0.223 ± 0.015	...	1.3E−03	1

Notes.—Col. (1): Names. Col. (2): Instrument. Col. (3): Wavelength (in μm). Cols. (4) and (5): Measured flux density and uncertainty (in Jy) at the specific wavelength. On the infrared flux density values in col. (5) color correction was applied. No color correction was applied on submillimeter fluxes. Col. (6): Quality of flux density, if available. Col. (7): Predicted flux density of the stellar photosphere (in Jy) at the specific wavelength. For a detailed description of the prediction method, see § 2.1. Col. (8): References for papers related to the quoted flux and its uncertainty in cols. (4) and (5).

[a] No quoted flux uncertainty in the *IRAS* Serendipitous Survey Catalog. We assumed $\delta F_{25} = 0.15$ Jy and $\delta F_{60} = 0.32$ Jy (4% relative uncertainty in both cases).

References.—(1) P. Ábrahám et al. 2006, in preparation; (2) http://data.spitzer.caltech.edu/popular/feps/20051123_enhanced_v1, FEPS Data Explanatory Supplement v3.0, Hines et al. 2005; (3) Kleinmann et al. 1986; (4) Moshir et al. 1989; (5) A. Moór et al. 2006, in preparation; (6) Rieke et al. 2005; (7) Chen et al. 2005b; (8) Williams et al. 2004; (9) Greaves et al. 2000; (10) Liu et al. 2004.

Decin et al. [2000] derived significantly higher values at 60 μm; the probable explanation is that we used a more advanced version, ver. 10.0, of the PIA software).

As was discussed in § 2.1, during the analysis we rejected several systems as bogus disks or suspicious objects. Those rejected stars that were previously proposed to harbor debris disks in the literature and would have been included in our final list (on the basis of their quoted fractional luminosity in the original paper) are presented in Appendix A, together with a brief description of the reason of rejection.

3. AGE DETERMINATION

3.1. *Membership in Young Moving Groups*

Age determination for main-sequence field stars is challenging and sometimes results in very uncertain values. Ages of open cluster members, however, can be estimated more accurately, e.g., by fitting their main-sequence locus in the color-magnitude diagram (CMD) with theoretical isochrones or by determining the location of the "lithium depletion edge" in the cluster and comparing it with the predictions of theoretical evolutionary models. A number of young clusters (α Per, Pleiades, Hyades, etc.) have been dated so far (Meynet et al. 1993; Stauffer et al. 1998). Similarly, the ages of young stellar kinematic groups, discovered mainly in recent years, are relatively well determined (e.g., Zuckerman & Song 2004b). It was a very important result that several stars with the strongest infrared excess turned out to be members of such moving groups, and in some cases the ages of these stars had to be revised significantly (e.g., the case of β Pic; Barrado y Navascués et al. 1999). In order to obtain more reliable ages for our sample, we performed a systematic investigation of the possible relationship between our excess stars and nearby kinematic moving groups, stellar associations, or open clusters.

A common method to decide whether an object belongs to a moving group is to compare its Galactic space velocity components with the mean velocity components of the group. In order to compute the space velocity for the stars in Table 1, we collected parallaxes and proper motions from the *Hipparcos* and Tycho-2 catalogs. When accurate parallax information was not available, a photometric distance was adopted.

Radial velocities were taken from the literature (see Table 3 for references) or from our own observations. The new observations were carried out with the 2.3 m ANU telescope at the Siding Spring Observatory, Australia, on 11 nights between 2005 March 21 and August 22. The spectra were taken with the Double Beam Spectrograph using a 1200 mm^{-1} grating in the red arm. The recorded spectra covered 1000 Å between 5800 and 6800 Å, with a dispersion of 0.55 Å $pixel^{-1}$. This leads to a nominal resolution of about 1 Å. The exposure time ranged between 30 and 200 s depending on the brightness of the target and the weather conditions. We obtained on average four to seven spectra for each star. Since all of the target stars are bright objects ($V < 10$ mag), we could easily reach S/N $\sim$ 150–200 for every spectrum. All spectra were reduced with standard tasks in IRAF.[10] Reduction consisted of bias and flat-field corrections, aperture extraction, wavelength calibration, and continuum normalization. We did not attempt flux calibration because the conditions were often nonphotometric and the main aim was to measure radial velocities. Radial velocities were determined by cross-correlation, using the IRAF task `fxcor`, choosing HD 187691 as a stable IAU velocity standard. The cross-correlated region was 100 Å centered on the Hα line, which is by far the strongest spectral feature in our range. The finally adopted velocities were calculated as simple mean values of the individual measurements. Our experiences have shown that the typical measurement errors were about 4–7 km s^{-1} per point, so that the mean values have $\pm$1–3 km s^{-1} standard deviations. These were adopted as the uncertainties shown in Table 3.

In the calculation of the Galactic space velocity we used a right-handed coordinate system (U is positive toward the Galactic center, V is positive in the direction of Galactic rotation, and W is positive toward the north Galactic pole) and followed the general recipe described in the *Hipparcos* and Tycho catalogs (ESA 1997). The computed Galactic space velocity components and their uncertainties are given in Table 3.

Table 4 summarizes the basic properties of the relevant moving groups and associations within 120 pc from the Sun. The probability that star i is a member of moving group j can be computed by

$$P_{ij} = \exp\left\{-\left[\frac{(U_i - U_j)^2}{2\left(\sigma_{U_i}^2 + \sigma_{U_j}^2\right)} + \frac{(V_i - V_j)^2}{2\left(\sigma_{V_i}^2 + \sigma_{V_j}^2\right)} + \frac{(W_i - W_j)^2}{2\left(\sigma_{W_i}^2 + \sigma_{W_j}^2\right)}\right]\right\}, \quad (2)$$

where U_i, V_i, W_i and σ_{U_i}, σ_{V_i}, σ_{W_i} are the Galactic space velocity components of the star and their uncertainties, respectively, while U_j, V_j, W_j and σ_{U_j}, σ_{V_j}, σ_{W_j} are the mean Galactic space velocity components of the specific kinematic group and the corresponding errors. In this formula we assumed that the velocity distribution within a group is Gaussian. When σ_{U_j}, σ_{V_j}, σ_{W_j} parameters were not available in the literature, we computed them from the velocity dispersion of known members around the mean. Our newly calculated mean values were always consistent with those from the literature within the uncertainties. In those few cases where no sufficient membership information could be found in the literature, we adopted $\sigma_{U_j} = \sigma_{V_j} = \sigma_{W_j} = 2$ km s^{-1} (a characteristic value in the previous cases).

Probability values for each star with respect to each group were computed. Then we checked the resulting P_{ij} values for objects already assigned to a group in the literature. The numbers spread in the range of $0.2 < P < 1.0$; therefore, we set $P = 0.2$ as a lower limit for the new moving group member candidates as well. Stars assigned to any group above this threshold were further checked by comparing their three-dimensional space location with the volume occupied by the group (most groups are rather confined in space). There were a few stars that could be assigned to both the Tucana-Horologium and GAYA2 associations; these cases are analyzed in Appendix B. Table 3 presents the final assignments between stars and kinematic groups.

From our sample of 60 objects, 26 sources could be linked to stellar associations; 13 of them are new members identified in the present study. For 10 stars out of these 13, age estimates are available in the literature. For these 10 objects we directly compare our age estimates with previous values in Table 5. In most cases ages derived in our study are younger than the earlier values. The discrepancy is particularly obvious in the case of ages derived from isochrone fitting (e.g., Nordström et al. 2004). However, this problem is not related only to the present study. For example, HD 105 has a moving group age of 30^{+10}_{-20} Myr (Mamajek et al. 2004), while Nordström et al. (2004) quoted 8600^{+4000}_{-3800} Myr from isochrone fitting. Similar objects in our sample are HD 25457 (50–100 Myr from moving group, Zuckerman & Song 2004b; 4000^{+1200}_{-2100} Myr from isochrones, Nordström et al. 2004), HD 164249 (12^{+8}_{-4} Myr, Song et al. 2003; 2200^{+1200}_{-1800} Myr, Nordström et al. 2004), and HD 181327 (12^{+8}_{-4} Myr, Song et al. 2003; 1300^{+1000}_{-1300} Myr, Nordström et al. 2004). The age uncertainty related to isochrone fitting might arise from the lack of information on whether the star is in the pre–main-sequence phase of its evolution or is an evolved object above the main sequence. In ambiguous cases we always adopted age estimates derived from stellar kinematic group membership.

3.2. *Statistical Age Estimates for the Disk Sample*

For stars not assigned to any moving groups, other age estimation methods are needed. Before focusing on individual systems, in this subsection we analyze what can be learned about the age distribution of our sample of debris disk systems.

3.2.1. *Distribution of the Excess Stars in the Velocity Space*

The distribution of the derived Galactic space velocities (Table 3) is displayed in Figures 1*a* and 1*b*. Overplotted is the box occupied by young disk population stars defined by Leggett (1992) on the basis of a systematic study of Eggen (1989). The plots show that most stars from our sample belong to this population. This fact suggests that the majority of our sample of stars from Table 1 are relatively young.

3.2.2. *Location of A-Type Stars on the CMD*

For a sample of bright A-type stars Jura et al. (1998) demonstrated that three objects with strong infrared excess (HR 4796A, HD 9672, β Pic) are located close to the lower boundary of the distribution in the CMD. Comparing their locations with the loci

[10] IRAF is distributed by the National Optical Astronomy Observatory, which is operated by the Association of Universities for Research in Astronomy, Inc., under cooperative agreement with the National Science Foundation.

TABLE 3
RADIAL VELOCITY INFORMATION AND MEMBERSHIP IN MOVING GROUPS

Name (1)	V_{rad} (km s^{-1}) (2)	References (3)	U (km s^{-1}) (4)	V (km s^{-1}) (5)	W (km s^{-1}) (6)	Association SKG (7)	Probability (%) (8)	References (9)
HD 105	+1.6 ± 0.3	1	−9.8 ± 0.4	−21.5 ± 0.8	−1.3 ± 0.3	TucHor	78	10
HD 377	+1.3 ± 0.3	1	−14.4 ± 0.6	−7.0 ± 0.4	−3.9 ± 0.3	...	...	11
HD 3003	+7.0 ± 2.0	2	−9.6 ± 0.8	−20.9 ± 1.0	−0.6 ± 1.6	TucHor	85	11
HD 6798	+10.0 ± 4.3	3	−36.6 ± 2.7	−13.5 ± 3.5	+4.1 ± 1.3	...	...	...
HD 8907	+8.8 ± 0.4	1	−10.4 ± 0.3	−4.6 ± 0.4	−16.7 ± 0.4	...	...	...
HD 9672	+11.4 ± 1.8	3	−23.9 ± 1.1	−16.6 ± 0.8	−6.6 ± 1.7	...	...	...
HD 10472	+19.5 ± 1.6	4	−8.5 ± 0.7	−24.2 ± 1.1	−10.4 ± 1.3	LA	38	4
HD 10647	+27.5 ± 0.2	1	−1.2 ± 0.1	−26.6 ± 0.2	−17.8 ± 0.2	...	...	...
HD 10638	−0.4 ± 1.2	5	−12.3 ± 1.0	−25.0 ± 1.5	−14.8 ± 1.0	LA	29	4
HD 15115	+8.8 ± 3.0	4	−13.2 ± 1.9	−17.8 ± 1.2	−6.0 ± 2.3	BPMG	22	4
HD 15745	+10.5 ± 1.2	4	−16.5 ± 1.1	−10.8 ± 1.3	−10.7 ± 0.7	...	...	...
HD 16743	+21.9 ± 1.1	4	−23.6 ± 0.9	−18.0 ± 0.6	−15.1 ± 0.9	...	...	...
HD 17390	+7.2 ± 1.8	1	−15.3 ± 0.8	−9.6 ± 0.5	+1.0 ± 1.6	...	...	...
HD 21997	+17.3 ± 0.8	3	−12.9 ± 0.5	−22.3 ± 1.0	−3.9 ± 0.9	GAYA2	62	4
HD 24966	+29.6 ± 2.2	4	−15.0 ± 0.9	−26.4 ± 1.4	−13.2 ± 1.8	...	...	...
HD 25457	+17.6 ± 0.2	1	−7.9 ± 0.2	−28.7 ± 0.4	−11.9 ± 0.2	AB Dor	30	12
HD 30447	+21.3 ± 2.5	4	−13.1 ± 1.4	−20.9 ± 1.6	−3.8 ± 1.7	GAYA2	54	4
HD 32297	+21.8 ± 2.1	4	−16.3 ± 2.0	−16.0 ± 1.5	−11.0 ± 1.0	...	...	...
HD 35841	+23.1 ± 1.3	4	−13.0 ± 1.0	−21.3 ± 1.7	−3.6 ± 1.7	GAYA2	56	4
HD 37484	+23.0 ± 2.6	4	−11.6 ± 1.4	−20.4 ± 1.9	−5.2 ± 1.3	TucHor	25	4
HD 38207	+24.9 ± 1.4	4	−14.7 ± 1.1	−21.2 ± 1.5	−4.1 ± 1.5	GAYA2	32	4
HD 38206	+24.9 ± 0.6	3	−13.7 ± 0.5	−21.2 ± 0.5	−6.1 ± 0.4	GAYA2	27	4
HD 38678	+18.9 ± 2.7	3	−13.6 ± 2.0	−10.5 ± 1.6	−8.1 ± 1.0	Castor	28	13
HD 39060	+20.2 ± 0.4	6	−10.9 ± 0.1	−16.2 ± 0.3	−9.2 ± 0.2	BPMG	98	14
HD 50571	+22.2 ± 1.2	1	−16.2 ± 0.4	−22.3 ± 1.1	−4.4 ± 0.5	...	...	...
HD 53143	+21.9 ± 0.1	1	−25.5 ± 0.3	−18.1 ± 0.1	−15.2 ± 0.1	...	...	...
HD 54341	+47.4 ± 1.4	4	−16.5 ± 0.5	−44.0 ± 1.3	−8.7 ± 0.5	...	...	...
HD 69830	+29.8 ± 0.1	1	+28.9 ± 0.5	−60.9 ± 0.4	−10.1 ± 0.2	...	...	...
HD 76582	−4.0 ± 2.5	5	+10.7 ± 1.8	+5.1 ± 1.1	+9.9 ± 1.5	...	...	...
HD 78702	+16.9 ± 2.1	3	−27.5 ± 1.6	−10.5 ± 1.8	−7.3 ± 1.1	...	...	...
HD 84870A	+3.7 ± 0.4	4	−7.8 ± 0.5	−25.5 ± 2.0	−5.7 ± 0.7	...	...	...
HD 85672	−5.2 ± 6.8	7	−9.5 ± 4.2	−3.0 ± 1.6	−14.8 ± 5.4	...	...	...
HD 92945	+22.6 ± 0.2	1	−15.2 ± 0.3	−27.8 ± 0.2	−4.3 ± 0.3	...	...	...
HD 107146	+1.5 ± 0.2	1	−10.6 ± 0.3	−28.8 ± 0.7	−5.2 ± 0.3	...	...	...
HD 109573A	+9.4 ± 2.3	3	−9.0 ± 1.3	−19.0 ± 1.9	−4.4 ± 1.0	TWA	64	15
HD 110058	+21.7 ± 1.3	4	+0.0 ± 1.3	−26.6 ± 1.4	−2.1 ± 0.8	...	...	...
HD 115116	−2.3 ± 0.7	7	−30.5 ± 1.5	−17.2 ± 1.1	−1.8 ± 0.3	...	...	...
HD 120534	+46.7 ± 1.1	4	+21.8 ± 1.8	−43.1 ± 3.2	+15.0 ± 1.8	...	...	...
HD 121812	−15.2 ± 0.7	8	−29.6 ± 1.2	−61.3 ± 2.7	−1.8 ± 0.9	...	...	...
HD 122106	−1.6 ± 5.0	1	+0.6 ± 2.6	−21.7 ± 2.0	−9.0 ± 4.2	...	...	...
HD 127821	−15.4 ± 2.6	1	−16.0 ± 0.5	−26.2 ± 1.6	−2.7 ± 2.0	...	...	...
HD 130693	+14.3 ± 0.8	4	+8.1 ± 0.9	−7.3 ± 0.6	+10.4 ± 0.8	...	...	...
HD 131835	+3.3 ± 1.7	4	−4.6 ± 1.6	−17.2 ± 2.1	−3.0 ± 1.0	UCL	50	16
HD 157728	−19.7 ± 1.2	5	−7.0 ± 0.8	−21.3 ± 0.8	−4.4 ± 0.6	...	...	...
HD 158352	−36.1 ± 1.2	5	−35.5 ± 1.1	−19.9 ± 0.5	+7.4 ± 0.9	...	...	...
HD 164249	−0.2 ± 0.5	1	−7.6 ± 0.6	−15.3 ± 0.7	−8.9 ± 0.4	BPMG	20	17
HD 169666	−44.3 ± 0.6	1	+1.3 ± 0.3	−46.8 ± 0.6	−7.9 ± 0.5	...	...	...
HD 170773	−26.3 ± 1.1	1	−30.5 ± 1.1	−3.8 ± 0.2	−12.3 ± 0.6	...	...	...
HD 172555	+2.0 ± 2.5	5	−11.0 ± 2.0	−15.6 ± 1.2	−9.3 ± 1.0	BPMG	96	17
HD 181296	−2.0 ± 10.0	2	−10.7 ± 8.6	−14.9 ± 2.7	−7.3 ± 4.4	BPMG	87	17
HD 181327	+0.2 ± 0.4	1	−9.1 ± 0.5	−16.2 ± 0.7	−8.4 ± 0.4	BPMG	57	17
HD 182681	+1.4 ± 5.0	9	−0.4 ± 4.6	−13.4 ± 1.1	−10.8 ± 1.8	...	...	...
HD 191089	−5.8 ± 2.2	1	−7.8 ± 1.9	−16.2 ± 0.9	−10.3 ± 1.2	BPMG	38	4
HD 192758	−11.1 ± 1.2	4	−18.4 ± 2.1	−13.8 ± 2.8	−6.7 ± 2.7	IC 2391	50	4
HD 197481	−4.5 ± 1.3	3	−10.1 ± 1.0	−16.4 ± 0.3	−10.5 ± 0.8	BPMG	56	14
HD 202917	−1.6 ± 0.2	1	−8.2 ± 0.4	−20.0 ± 1.1	−0.3 ± 0.2	TucHor	48	11
HD 205674	+1.1 ± 5.1	4	−1.6 ± 3.0	−24.5 ± 2.4	−16.6 ± 3.7	...	...	...
HD 206893	−12.9 ± 1.4	1	−20.0 ± 0.9	−7.7 ± 0.7	−2.1 ± 1.0	...	...	...
HD 218396	−12.6 ± 1.3	3	−12.4 ± 0.5	−21.4 ± 1.1	−7.4 ± 0.9	LA	62	4
HD 221853	−4.2 ± 2.1	4	−12.7 ± 0.9	−20.6 ± 1.8	−11.2 ± 1.9	LA	94	4

NOTES.— Col. (1): Names. Col. (2): Radial velocity and its uncertainty. Col. (3): References for the source of measurement. Cols. (4)–(6): U, V, W Galactic space velocity components; U is positive toward the Galactic center, V is positive in the direction of Galactic rotation, and W is positive toward the north Galactic pole. Col. (7): Assigned stellar kinematic group (see Table 4). Col. (8): Membership probability. Col. (9): References for membership identification.

REFERENCES.— (1) Nordström et al. 2004 and references therein; (2) Zuckerman & Webb 2000; (3) Kharchenko et al. 2004 and references therein; (4) this paper; (5) Wilson 1953; (6) Zuckerman et al. 2001a; (7) Grenier et al. 1999; (8) Strassmeier et al. 2000; (9) Evans 1967; (10) Mamajek et al. 2004; (11) Zuckerman et al. 2001b; (12) Zuckerman & Song 2004b; (13) Barrado y Navascués 1998; (14) Barrado y Navascués et al. 1999; (15) Webb et al. 1999; (16) de Zeeuw et al. 1999; (17) Song et al. 2003.

TABLE 4
Description of Stellar Kinematic Groups

Group Name (1)	U, V, W (km s^{-1}) (2)	References (3)	Age (Myr) (4)	References (5)
AB Dor moving group	−8, −27, −14	1	50	1
	...	...	100	6
β Pictoris moving group	−11, −16, −9	1	12^{+8}_{-4}	7
Castor moving group	−10.7, −8.0, −9.7	2	200 ± 100	2
Great Austral young association 2	−11.0, −22.5, −4.6	3	20	3
Hyades	−40, −17, −3	1	600	1
IC 2391 supercluster	−20.6, −15.7, −9.1	4	35–55	4
Local Association	−11.6, −21.0, −11.4	4	20–150	4
Lower Centaurus Crux	−8.2, −18.6, −6.4	5	16 ± 1	8
Upper Centaurus Lupus	−6.8, −19.3, −5.7	5	17 ± 1	8
Tucana/Horologium	−11, −21, 0	1	30	1
	...	...	10–30	9
	...	...	20	10
	...	...	10–40	11
TW Hydrae association	−11, −18, −5	1	8	1
	...	...	5–15	12
Ursa Major moving group	+14, +1, −9	1	300	1
	...	...	500	13

References.—(1) Zuckerman & Song 2004b and references therein; (2) Barrado y Navascués 1998; (3) Torres et al. 2003; (4) Montes et al. 2001 and references therein; (5) Sartori et al. 2003; (6) Luhman et al. 2005; (7) Zuckerman et al. 2001a; (8) Mamajek et al. 2002; (9) Stelzer & Neuhäuser 2000; (10) Torres et al. 2000; (11) Zuckerman et al. 2001b; (12) Weintraub et al. 2000; (13) King et al. 2003.

TABLE 5
Comparison of Age Estimates for Newly Identified Moving Group Members

Name	Age Estimates (Myr)	References
HD 10472	2000^{+1000}_{-1400}	1
	30	2
	[20, 150]	3
HD 15115	900^{+1300}_{-900}	1
	100	2
	12^{+8}_{-4}	3
HD 21997	100	2
	20^{+10}_{-10}	3
HD 30447	2100^{+700}_{-1100}	1
	≲100	2
	20^{+10}_{-10}	3
HD 37484	1500^{+900}_{-1500}	1
	[30, 100]	4
	30^{+10}_{-20}	3
HD 38207	[100, 300]	4
	20^{+10}_{-10}	3
HD 38206	$\sim 9^{+14}_{-9}$	5
	20^{+10}_{-10}	3
HD 191089	17^{+8}_{-4}	6
	3000^{+700}_{-900}	1
	≲100	2
	12^{+8}_{-4}	3
HD 218396	732^{+396}_{-682}	7
	30	2
	[20, 150]	3
HD 221853	800	8
	1800	9
	1700^{+500}_{-600}	1
	≲100	2
	[20, 150]	3

References.—(1) Nordström et al. 2004; (2) Zuckerman & Song 2004a; (3) this paper; (4) Carpenter et al. 2005; (5) Gerbaldi et al. 1999; (6) Mamajek 2004; (7) Song et al. 2001; (8) Silverstone 2000; (9) Decin et al. 2000.

of the youngest, nearby open clusters (α Per, IC 2391, Pleiades), Lowrance et al. (2000) argued that stars with strong infrared excess are typically younger than these clusters. Adopting this idea, we selected stars with $B - V$ ranging between −0.1 and 0.33 (corresponding mainly to A-type stars) from Table 1 and plotted them in the CMD of Figure 2. In addition, we overplotted a volume-limited sample of A-type stars ($d < 100$ pc) extracted from the *Hipparcos* catalog (it was requested that the parallax error was less than 10% and the $B - V$ uncertainty was lower than 0.01 mag). For comparison, members of the open clusters α Per (80 Myr) and Hyades (600 Myr) are marked. The older cluster, Hyades, covers the upper part of the distribution, while α Per stars are situated at lower absolute magnitudes for the same color. Pleiades (100 Myr, not plotted in the figure for clarity) occupies the same region as α Per (see Fig. 3 of Lowrance et al. 2000).

Figure 2 shows that the majority of the objects from our sample of high-f_d stars appear to be close to the lower boundary of the area occupied by A stars and are located below the region of α Per and Pleiades, with some overlap. This suggests that the early spectral type stars from our sample of high-f_d disks are young, probably close to the zero-age main sequence (ZAMS), and they are presumably not older than 100 Myr, the age of the Pleiades.

3.3. *Ages of Individual Objects*

For those objects that could be assigned to one of the moving groups or associations, the age of that group, as well as its uncertainty, was adopted (26 objects). For a number of stars not associated with groups or with associations, age estimates could be found in the literature (19 stars; for references see Table 1). Sometimes literature data for a specific star scatter significantly; in these cases we adopted an age range that covers all quoted values and their uncertainties. When the literature search did not yield any dating, we made age estimates by plotting the stars on the H-R diagram and comparing their positions to isochrones. For stars

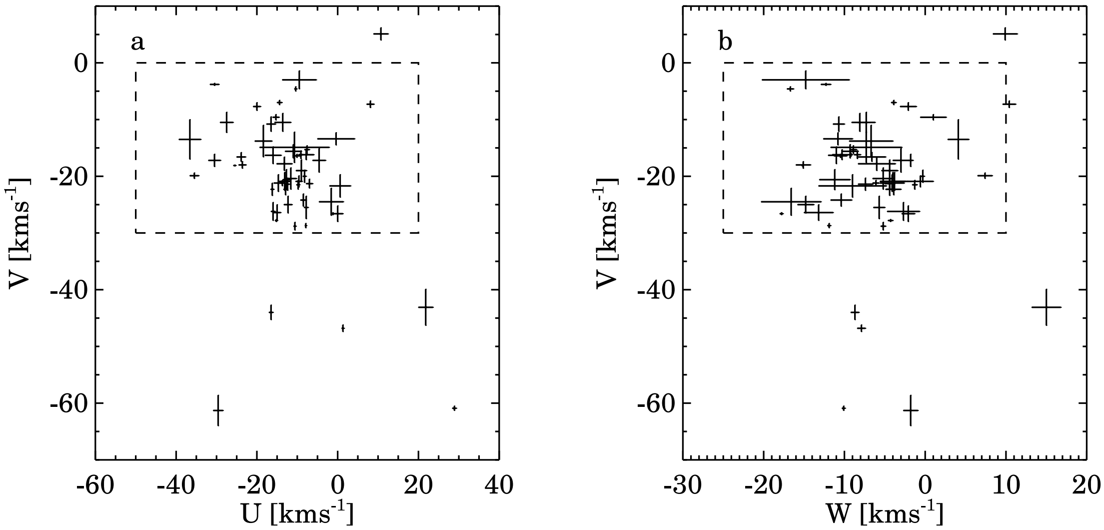

FIG. 1.—(U, V)- and (W, V)-planes for stars in Table 3. The dashed rectangle marks the young disk population as defined by Leggett (1992).

with spectral types in the range B9–G5 the isochrone age was estimated following the general outline described by Lachaume et al. (1999), using the Padova theoretical isochrones (Girardi et al. 2000). This method was applied to 13 objects.

This isochrone method gives only upper limits for some A-type stars. As a best estimate for these stars (five cases), we adopted an upper limit of 100 Myr, consistent with our results shown in Figure 2 and discussed in § 3.2.2. For stars of later spectral type there are some widely used age indicators, like the strength of the Ca II H and K lines or the X-ray luminosity of the star. In the case of HD 121812 our age estimate is based on the former method, taking the measured value from Strassmeier et al. (2000) and using the calibration of Lachaume et al. (1999). HD 130693 has a *ROSAT* counterpart and its X-ray luminosity of $\log L_X = 29.7$ ergs s^{-1} was compared with the X-ray luminosity distribution function of late-type members in different

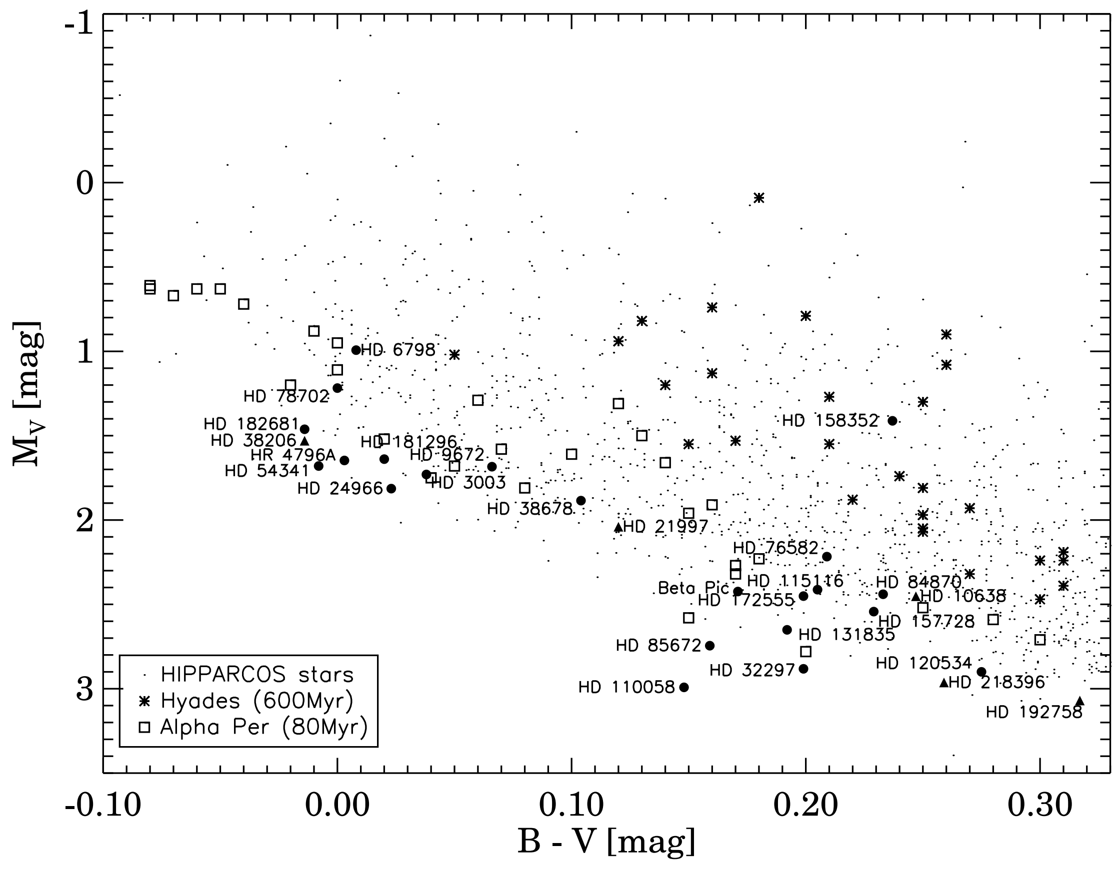

FIG. 2.—CMD of A-type stars. Objects measured by *Hipparcos* within 100 pc from the Sun with parallax error (<10%) and ($B-V$) error (<0.01 mag) are represented by small dots. Filled symbols mark positions of A- and F0-type stars from Table 1; triangles correspond to objects assigned to any stellar kinematic group in this work. Stars of α Per and Hyades open clusters are represented by squares and asterisks, respectively.

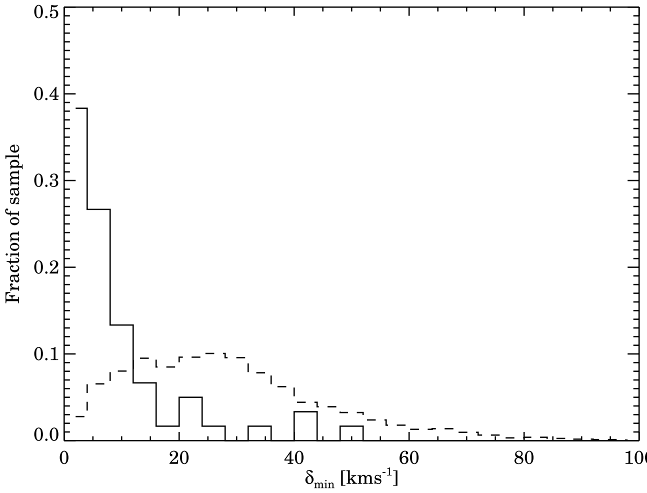

FIG. 3.—Histogram of distances in the three-dimensional velocity space to the closest moving group. *Solid line:* stars from Table 3; *dashed line:* volume-limited *Hipparcos* sample (see § 4.1).

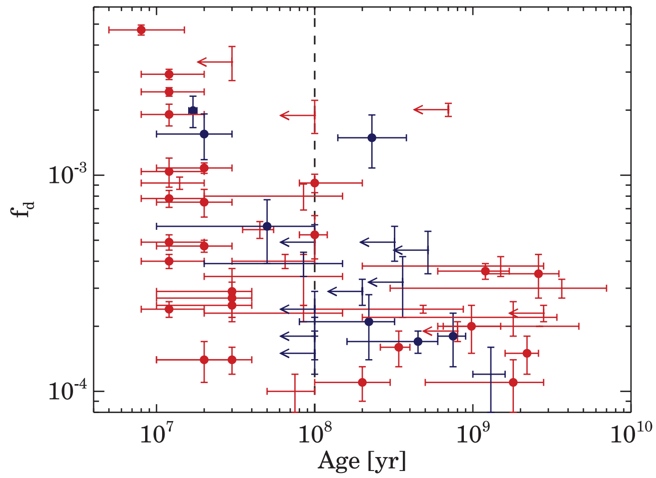

FIG. 4.—Fractional luminosity of the infrared excess as a function of age. *Dashed line:* threshold of 100 Myr. Upper age limits are denoted by arrows, whose hats correspond to the uncertainty in f_d. When only an age range is known, no filled circle was plotted. Red symbols mark those debris systems whose existence was explicitely confirmed by an instrument independent of *IRAS* (§ 4.2).

associations (see Fig. 2 of Stelzer & Neuhäuser 2000), yielding an age range of 10–100 Myr. In Table 1 we summarize the age estimates for each object.

4. DISCUSSION

4.1. *Connection between Debris Disks and Young Moving Groups*

From our sample of 60 main-sequence stars exhibiting strong infrared excess, 26 can be assigned to young stellar kinematic groups. In order to test whether the frequency of stars belonging to young stellar kinematic groups is similar in a general sample, we determined the corresponding ratio within a volume-limited sample of normal stars. First, we created this sample by selecting stars from the *Hipparcos* catalog using the following criteria: (1) they are closer than 120 pc (the same volume limit as in our sample), (2) their survey flag in the catalog[11] was set to "S," and (3) they have radial velocity measurement with uncertainty less than 5 km s^{-1}. The second condition guarantees that stars observed in various individual projects do not introduce a bias in the analysis of the velocity distribution (Skuljan et al. 1999). In addition, Binney et al. (1997) noted that radial velocities are preferentially observed for high proper motion stars, which may cause a kinematical bias in our sample. Following the proposal of Skuljan et al. (1999), we constrained the sample for stars exhibiting low transverse velocity and excluded all stars with $v_t \geq 80$ km s^{-1} in order to avoid this bias.

The query resulted in 7519 objects, for which we computed the *UVW* Galactic space motion components. For each star in the two samples (the 60 debris systems in Table 1 and the newly defined volume-limited stellar sample) we determined the Euclidean distance in the three-dimensional velocity space from the closest moving group, δ_{min}. In this analysis we considered only groups younger than 150 Myr. In Figure 3 we plotted the histograms of δ_{min} for the two samples. A two-sided Kolmogorov-Smirnov test shows that the two distributions are different with a probability higher than 99.99%. This result indicates that debris systems of high infrared fractional luminosity are much more intimately linked to the nearby young stellar kinematic groups than the majority of normal stars.

4.2. *The Relationship between Fractional Luminosity and Age*

Zuckerman & Song (2004b) hypothesized that stars with $f_d > 10^{-3}$ are younger than 100 Myr and therefore a high f_d value can be used as an age indicator. This proposal is in contradiction with the conclusion of Decin et al. (2003), who claimed the existence of high-f_d disks around older stars. In order to test which proposal is supported by our data, in Figure 4 we plotted the distribution of ages as a function of the fractional luminosity f_d from Table 1. We plotted in red the debris disks whose presence was explicitly confirmed by an instrument independent of *IRAS* (see col. [8] in Table 1). The confirmation could be based, e.g., on high spatial resolution infrared images (*ISO* ISOPHOT, *Spitzer* MIPS), on mid-infrared spectra (*Spitzer* IRS), or on coronagraphic images (*HST* ACS, *HST* NICMOS). We found 43 confirmed debris disks in total.

Most data points with $f_d > 5 \times 10^{-4}$ fall below the age threshold of 100 Myr (marked by a dashed line), while objects with lower f_d show a larger spread in age. This trend can be recognized in the whole sample but is especially clear in the confirmed subsample (*red symbols*). There is only one noteworthy case: HD 121812 with an age of 230^{+150}_{-90} Myr exhibits fractional luminosity exceeding the 5×10^{-4} threshold value. However, the presence of a debris disk around this star has not been confirmed independently of *IRAS*. On the basis of this result, we conclude that, according to the suggestion of Zuckerman & Song (2004b), the majority of debris disks with $f_d > 5 \times 10^{-4}$ are younger than 100 Myr, and high fractional luminosities can be used as an indicator of youth. Nevertheless, the opposite is not true, i.e., a low f_d value is not correlated with age and, in particular, is not an indicator of antiquity.

There is a growing list of debris disk systems that have been discovered by the sensitive detectors of the *Spitzer Space Telescope* (Beichman et al. 2005a; Bryden et al. 2006; Chen et al. 2005a, 2005b; Kim et al. 2005; Low et al. 2005; Meyer et al. 2004; Stauffer et al. 2005; Uzpen et al. 2005), and one may wonder whether these new observations support our previous

[11] Field H68 in the *Hipparcos* catalog. "S" indicates that the entry is contained within the "survey," which was the basic list of bright stars added to and merged with the total list of proposed stars, to provide a stellar sample almost complete to well-defined limits. The limiting magnitude was a function of the stars's spectral types and Galactic latitude.

conclusion. As a preliminary check we collected from the cited papers all debris disks with $f_d > 5 \times 10^{-4}$. We used fractional luminosity values and age estimates as quoted in the papers. We found that all of these new disks discovered so far belong to the ~16 Myr old Lower Centaurus Crux subgroup of the Scorpius-Centaurus association (HD 106906, HD 113556, HD 113766, HD 114082, HD 115600, HD 117214; Chen et al. 2005a), to the TWA (TWA 7, TWA 13A, TWA 13B; Low et al. 2005), or to the star-forming region RCW 49 (18 possible warm debris disks; Uzpen et al. 2005), which unambiguously shows that these objects are young, in agreement with the conclusion of the present paper.

4.3. *Debris Disk Evolution and the Cases of Old Systems*

There are a number of models in the literature (see § 1) to describe the temporal evolution of debris disks. In the following we compare our results with predictions.

Dominik & Decin (2003) proposed a simple collisional model that assumes that all dust grains in the debris disk are produced in collisions between planetesimals within a ring whose radius is constant during the whole evolution. In collisional equilibrium, when the dust production and destruction rates are in balance, the grain loss mechanism governs the amount of dust visible in the system. If dust destruction is dominated by collisions, the fractional luminosity f_d decreases proportionally to t^{-1}. If the dust removal process is dominated by the Poynting-Robertson drag, $f_d \propto t^{-2}$. It is predicted that in disks with $f_d > 10^{-4}$ the evolution is dominated by collisions (Dominik & Decin 2003; Wyatt 2005).

Three families of disk evolution models, computed from equations (7) and (35)–(40) of Dominik & Decin (2003), are plotted as shaded bands in Figure 5. The data points and symbols in this figure are identical to those in Figure 4. The main differences between the model families are related to disk mass: (1) $M_d = 10\ M_\oplus$, (2) $M_d = 50\ M_\oplus$, and (3) $M_d = 250\ M_\oplus$. The width of each band corresponds to a range in stellar mass from 0.5 to 3 $M_\odot$. Additional parameters are the characteristic radius of the ring of planetesimals $r_c = 43$ AU, the radius of planetesimals $a_c = 10$ km, the density of the planetesimal material $\rho_c = 1.5$ g cm^{-3} (proposed for icy bodies with a small rocky component; Greenberg 1998; Kenyon 2002), the size of the smallest visible grains $a_{\rm vis} = 10\ \mu$m (taken from Jura et al. 2004), the absorption efficiency of the dust particles $Q_{\rm abs} = 1$, and $\epsilon_0 = 226$ (defined in eq. [22] of Dominik & Decin 2003).

Figure 5 shows that the location of most stars on the evolutionary diagram can be explained by the models. The number of older stars exhibiting high f_d values incompatible with the models is relatively low. Most of these disks are located in the $t \geq 10^9$ yr and $f_d \lesssim 5 \times 10^{-4}$ area. A possible explanation for the origin of these stars was proposed by Dominik & Decin (2003), who assumed that different planetesimal disks become active debris systems at different ages because of the delayed onset of the collisional cascade. Large collisional events may also increase the brightness of a debris disk temporarily (Rieke et al. 2005). Extraordinary events during the evolution like, e.g., a proposed "supercomet" in the HD 69830 system (Beichman et al. 2005b) cannot be excluded either. Nevertheless, the low number of systems incompatible with the models, especially at $f_d \gtrsim 5 \times 10^{-4}$, indicates that the above scenarios do not represent the main evolutionary trend.

It is important to note that a large spread in fractional luminosities ($10^{-4} < f_d < 5 \times 10^{-3}$) can be observed in the figure among young debris systems ($t < 100$ Myr). This result resembles the findings of Rieke et al. (2005) among A-type stars but somewhat contradicts those of Decin et al. (2003) and Dominik & Decin (2003), who found only a few young stars with moderate or small infrared excesses and proposed that it might be related to the effect of stirring. A possible explanation of the large spread among young stars could be that the initial conditions of the disks (especially initial disk mass) are far from being homogeneous.

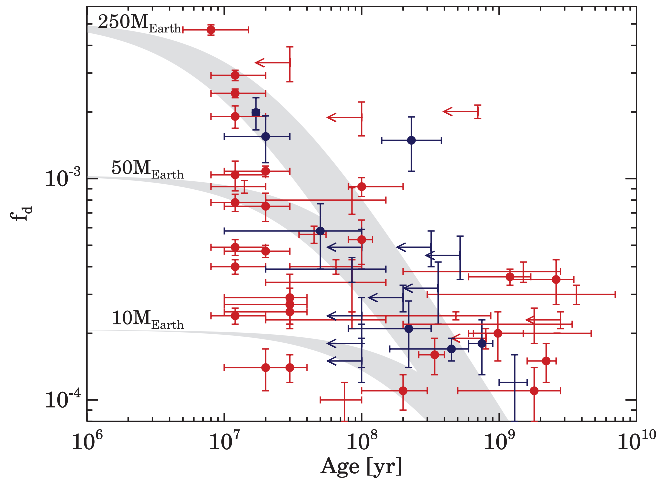

FIG. 5.—Fractional luminosity of the infrared excess as a function of age. The shaded bands mark the evolutionary models of Dominik & Decin (2003; for detailed model parameters see § 4.3). Upper age limits are denoted by arrows, whose hats correspond to the uncertainty in f_d. When only an age range is known, no filled circle was plotted.

5. CONCLUSIONS

We searched the *IRAS* and *ISO* databases and compiled a list of debris disks exhibiting the highest fractional luminosity values ($f_d > 10^{-4}$) in the vicinity of the Sun ($d < 120$ pc). Utilizing high-resolution far-infrared maps, we attempted to exclude bogus disks from the sample. We recomputed the fractional luminosity value for each disk using available *IRAS*, *ISO*, and *Spitzer* data and analyzed the Galactic space velocities of the objects, as well as the distribution of the disks on the fractional luminosity versus age diagram. Our results are summarized as follows:

1. We compiled a list of 60 debris disk systems of high fractional luminosity. Eleven of them are new discoveries, and 4 out of these 11 have been confirmed by *Spitzer* observations.
2. Disks with high fractional luminosity often belong to young stellar kinematic groups, providing an opportunity to obtain improved age estimates for these disks.
3. Practically all objects with $f_d > 5 \times 10^{-4}$ are younger than 100 Myr.
4. The number of old systems with high f_d seems to be lower than was claimed before, mainly as a consequence of the age revision in connection to the young stellar kinematic groups.
5. There exist many young disks of moderate fractional luminosity.
6. Comparing the theoretical evolutionary model of Dominik & Decin (2003) with the observations in the f_d versus age diagram, good general agreement was found.

We are grateful to the anonymous referee for his/her comments that improved the paper.

This research has made use of the *IRAS* and *Hipparcos* catalogs (ESA 1997), as well as the SIMBAD database and the VizieR tool operated by CDS, Strasbourg, France. The Two Micron All

Sky Survey (2MASS) is a joint project of the University of Massachusetts and the Infrared Processing and Analysis Center/California Institute of Technology, funded by the National Aeronautics and Space Administration and the National Science Foundation.

This work is based on observations made with the *Spitzer Space Telescope*, which is operated by the Jet Propulsion Laboratory, California Institute of Technology under a contract with NASA. Support for this work was provided by NASA through an award issued by JPL/Caltech.

This material is partly based on work supported by the National Aeronautics and Space Administration through the NASA Astrobiology Institute under Cooperative Agreement CAN-02-OSS-02 issued through the Office of Space Science.

The *ISO* Data Archive is maintained at the *ISO* Data Centre, Villafranca, Madrid, and is part of the Science Operations and Data Systems Division of the Research and Scientific Support Department. ISOPHOT observations were reduced using the ISOPHOT Interactive Analysis package PIA, which is a joint development by the ESA Astrophysics Division and the ISOPHOT Consortium, led by the Max-Planck-Institut für Astronomie (MPIA).

The work was partly supported by grants OTKA K62304 and T043739 of the Hungarian Scientific Research Fund.

APPENDIX A

BOGUS DEBRIS DISKS

In the last few years several *IRAS*-based debris disk candidates turned out to be bogus. Examples are HD 155826 (Lisse et al. 2002), or the list of Kalas et al. (2002). The most common problems are contamination by background objects (cirrus knots, galaxies), Pleiades-like nebulosity, or unreliable point-source detection by *IRAS*. Our list of debris disk candidates is based on *IRAS* data; however, when higher resolution far-infrared observations were available, we checked whether the above-mentioned problems could have affected the detection of the disk. In Table 6 we list those objects that were identified as debris systems in the literature (and claimed to have $10^{-4} < f_d < 10^{-2}$ in the original paper) but that our analysis indicates are very likely bogus disks. In the following we briefly describe the reason of rejection.

HD 34739.—The source position in the MIPS 70 μm map differs from the star's position by 26″ but coincides with the near-infrared source 2MASS J05163646−5257397 with an offset of 2″.

HD 53842.—This system is not a real bogus disk, since at 24 μm the star shows infrared excess (A. Moór et al. 2006, in preparation), but at 70 μm the IR emission comes from an independent compact source separated by 19″. This nearby source coincides with 2MASS J06460135−8359359, within a distance of 2″. Due to this fact, the fractional luminosity of HD 53842 decreased below our lower limit.

HD 56099.—The source position in the MIPS 70 μm map differs from the star's position by 24″ but coincides with the near-infrared source 2MASS J07190966+5907219 with an offset of 2″.

HD 72390.—The peak brightness position in the ISOPHOT maps at 60 and 90 μm differs from the stellar position by 36″. Coordinates of this peak are very close to those of 2MASS J08143635−8423260, which is an extended 2MASS source (XSC 1524951), with an offset of 5″.

TABLE 6

List of Bogus Disks

Name (1)	Nearby *IRAS* Source (2)	First Reference as Debris Disk Candidate (3)	Reason of Rejection (4)	Instrument (5)	Position of Unrelated Nearby IR Source: R.A. (J2000.0) (6)	Position of Unrelated Nearby IR Source: Decl. (J2000.0) (7)
HD 23484	F03423−3826	1[a]	No detectable excess[a]	ISOPHOT	...	...
HD 34739	F05154−5301	1	Source confusion	MIPS	05 16 36.3	−52 57 40
HD 53842	F06539−8355	2	Source confusion[b]	MIPS	06 46 02.8	−83 59 37
HD 56099	F07149+5913	1	Source confusion	MIPS	07 19 09.6	+59 07 20
HD 72390	F08210−8414	1	Source confusion	ISOPHOT	08 14 39	−84 23 23
HD 82821	F09319+0346	1	Source confusion	MIPS	09 34 36.2	+03 32 39
HD 143840	F16001−0440	1	Extended emission	ISOPHOT, MIPS	...	...
HD 158373	F17265−0957	1[a]	No detectable excess[a]	ISOPHOT	...	...
HD 164330	F17559+6236	1[a]	No detectable excess[a]	ISOPHOT	...	...
HD 185053	F19415−8123	1	Extended emission	MIPS	...	...
HD 204942	F21297−2422	1	Source confusion	MIPS	21 32 35.8	−24 09 30

Notes.—Col. (1): Name. Col. (2): Identification of nearby *IRAS* source. The *IRAS* source is always located within 30″ of the star position. Col. (3): Reference for first mention as debris disk candidate. Col. (4): Reason why the object was classified as a bogus disk and rejected from further analyses. Col. (5): Instrument. Cols. (6) and (7): Units of right ascension are hours, minutes, and seconds, and units of declination are degrees, arcminutes, and arcseconds. When the object was nominated as a bogus disk due to source confusion, position of the unrelated nearby IR source is given. In the cases of MIPS observations MOPEX was used to extract source coordinates from 70 μm MIPS images. The coordinates of peak brightness in ISOPHOT maps were determined by fitting a point-source profile.

[a] Silverstone (2000) selected these objects as debris disk candidates on the basis of *IRAS* data, but found that ISOPHOT observations did not confirm the detection of IR excess. He proposed that the nondetection of far-infrared flux excess toward the star's position can be explained by cirrus contamination.

[b] HD 53842 is not really bogus. At 24 μm it shows IR excess above the photosphere (see A. Moór et al. 2006, in preparation). However, at 70 μm the excess emission is related to a nearby infrared source.

References.—(1) Silverstone 2000; (2) Mannings & Barlow 1998.

TABLE 7
LIST OF REJECTED SUSPICIOUS OBJECTS

Name (1)	Nearby *IRAS* Source (2)	First Reference as Debris Disk Candidate (3)	Reason of Suspicion (4)	Name of Background Source (5)
HIP 13005	F02444+1505	1	Nearby extended 2MASS source[a]	2MASS J02471368+1518315 (XSC 122165)
HD 33095	F05049−1927	1	Cirrus	...
HD 36162	F05275+1519	1	Nearby extended 2MASS source	2MASS J05303093+1521513 (XSC 2620748)
HD 39944	F05526−2535	2	Nearby galaxy[b]	ESO 488-41
HD 83870	F09393+4111	1	Nearby galaxy	PGC 27759
HD 97455	F11107+5541	1	Nearby galaxy	PGC 34197
HD 124718	F14129−2707	1	Nearby 2MASS source with an excess in the K_s band	2MASS J14155109−2721050
HD 140775	F15429+0536	1	Star locates in the wall of Local Bubble or beyond	...
HD 154145	F17011−0004	1	Star locates in the wall of Local Bubble or beyond	...

NOTES.—Col. (1): Name. Col. (2): Identification of nearby *IRAS* source. The *IRAS* source is always located within 30″ of the star position. Col. (3): Reference for first mention as debris disk candidate. Col. (4): Reason of suspicion. For more details see § 2.3. Col. (5): Name of background source.

[a] Zuckerman & Song (2004a) also found suspicious this debris candidate based on the offset between its *IRAS* positions measured at 12 and 60 μm.

[b] Sylvester & Mannings (2000) also noted this coincidence between the position of the *IRAS* source and the nearby galaxy.

REFERENCES.—(1) Silverstone 2000; (2) Mannings & Barlow 1998.

HD 82821.—We have detected two infrared sources in the MIPS 70 μm map, but their positions significantly differ from the position of the star. The position of the brighter one lies at 70″ from the nearby *IRAS* source (FSC 09319+0346) and is located just outside the 2 σ error ellipse (nearly along the major axis) but well inside the 3 σ error ellipse. We assume that this source, whose position coincides well with the near-infrared source 2MASS J09343630+0332417 (XSC 2391850) within a distance of 3″, is responsible for the source confusion. The second source was probably below the *IRAS* sensitivity limit.

HD 143840.—ISOPHOT minimap observation at 90 μm and a *Spitzer* MIPS image at 70 μm show extended IR emission. The image of the Digitized Sky Survey also shows a reflection nebulosity around this star. We think that the excess far-infrared emission comes from the nebula.

HD 185053.—Magakian (2003) proposed that HD 185053 is the illuminating source of the reflection nebula GN 19.41.5. *Spitzer* MIPS observations at 24 and 70 μm show extended IR emission around the star. We think that the excess far-infrared emission is related to the nebula rather than to a debris disk.

HD 204942.—The source position in the MIPS 70 μm map differs from the star's position by 22″ but coincides with the near-infrared source 2MASS J21323602−2409319 with an offset of 4″.

HD 23484, HD 158373, and HD 164330.—ISOPHOT minimap observations of these stars at 60 and 90 μm did not show excess above the photosphere. This discrepancy between the *IRAS*-based excesses and the nondetection of excesses by ISOPHOT (which had better spatial resolution than *IRAS* at far-infrared wavelengths) was already mentioned by Silverstone (2000), who suggested cirrus contamination as the reason.

For stars when no higher resolution data were available a set of criteria were applied to filter out suspicious objects that might be bogus disks (see § 2.3). In Table 7 we listed those objects that were earlier identified as debris disks in the literature (with $10^{-4} < f_d < 10^{-2}$) but were rejected from further analysis according to our criteria. Nevertheless, future high spatial resolution infrared data are needed to prove or disprove our judgment.

APPENDIX B

NEW MEMBERS IN THE YOUNG STELLAR KINEMATIC GROUPS

β Pictoris moving group (*BPMG*).—We identified two stars that are candidate members of this group: HD 15115 and HD 191089. HD 15115 is a northern object. Although the first surveys found BPMG members only in the southern hemisphere (Barrado y Navascués et al. 1999; Zuckerman et al. 2001a), recently Song et al. (2003) proposed several new northern candidates. One of those, HIP 12545, is located within 4° to HD 15115 on the sky. HD 15115 has a *ROSAT* counterpart with fractional X-ray luminosity of $\log(L_X/L_{bol}) = -4.94$ ($\log L_X = 29.2$ ergs s^{-1}). These properties are comparable to those of stars with similar mass in young star associations (see Figs. 9 and 10 of de la Reza & Pinzón 2004).

HD 191089 is somewhat more distant (see Table 1) than known members of the group in the list of Zuckerman & Song (2004b). However, a large part of this list is based on a volume-limited survey within $d < 50$ pc, and other authors proposed candidates at larger distances (Torres et al. 2003). HD 191089 shows several signs of youth. Mamajek (2004) classified this star as younger than Pleiades because its lithium abundance [EW(Li) = 95 ± 6 mÅ] was higher than 95% of Pleiades stars with similar effective temperatures. Isochronal age of the star (17^{+8}_{-4} Myr; Mamajek 2004) is in good agreement with the age of the β Pictoris moving group (12^{+8}_{-4} Myr; see Table 4). Moreover, HD 191089 rotates rapidly compared with typical F5-type stars ($v \sin i = 45$ km s^{-1}; Nordström et al. 2004). It has a *ROSAT* X-ray luminosity of $\log L_X = 29.2$ ergs s^{-1} and X-ray fractional luminosity of $\log(L_X/L_{bol}) = -4.93$. These values are also comparable with the properties of stars with similar spectral types in nearby kinematic groups (see Figs. 9 and 10 of de la Reza & Pinzón 2004).

The GAYA2 and TucHor associations.—The Great Austral young association 2 (GAYA2) and Tucana/Horologium (TucHor) association can be discussed together since they overlap both in their location on the projected sky plane and in velocity space. GAYA2

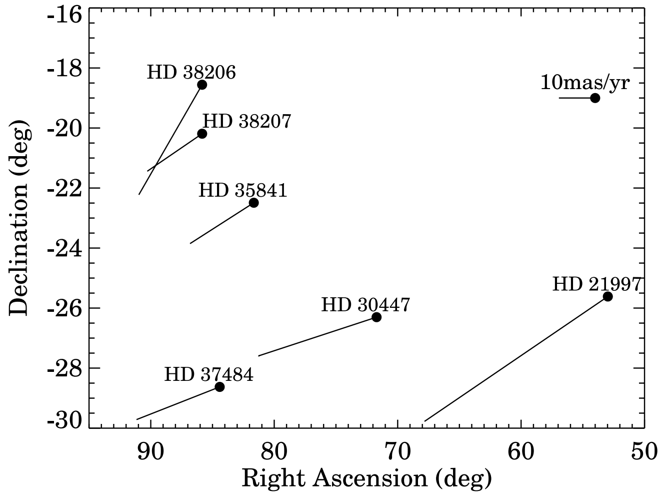

FIG. 6.—Positions and proper motions of proposed new members of the Tucana-Horologium and GAYA2 associations (see Appendix B).

was discovered in the framework of the SACY (Search for Associations Containing Young stars) survey (Torres et al. 2003), and the known members are confined mostly in the right ascension (R.A.) range $3^h < \text{R.A.} < 9^h$. Recently identified members of TucHor occupy a similar region ($2^h < \text{R.A.} < 7^h$), and several of them show only slightly different Galactic space motions compared to the mean *UVW* velocities of the Tucana nucleus and resemble the mean space motions of GAYA2. Although GAYA2 is more distant (located at a mean distance of ~84 pc, while TucHor members located in the same sky region have a mean distance of ~50 pc), there is an overlap in radial distance, as well. Studying the relationship between the two associations is beyond the scope of this work. As a practical solution, we assigned all doubtful sources (see Fig. 6) of $D \leq 67$ pc to the TucHor association and the more distant ones to GAYA2. Thus, we propose that one of these sources, HD 37484, belongs to TucHor (its space velocity is not inconsistent with that of other neighboring TucHor members). The measured lithium abundance of the star (Favata et al. 1993) is a strong indication of its youth. HD 21997, HD 30447, HD 35841, HD 38206, and HD 38207 are classified as members of the GAYA2 group. It is worth mentioning that these five stars form a spectacular concentration of high-f_d debris disks within a relatively small area on the sky.

Local Association.—We propose that HD 10472, HD 10638, HD 218396, and HD 221853 belong to the Local Association. HD 10472 was previously a TucHor candidate (Torres et al. 2000; Zuckerman et al. 2001b), but recently Zuckerman & Song (2004b) suggested that its membership status is uncertain; thus, it may be consistent with our result.

IC 2391 supercluster.—On the basis of its Galactic space velocity HD 192758 may belong to the IC 2391 supercluster. Its position on the CMD (see Fig. 2 and § 3.2.2) also suggests its youth.

HD 110058.—This was earlier classified as a member of the Lower Centaurus Crux (LCC) association using the convergent point method (de Zeeuw et al. 1999). However, according to our results, its Galactic space velocity is inconsistent with the mean velocity of the LCC. Nevertheless, HD 110058 seems to be a very young object on the basis of its position on the CMD of A-type stars (see § 3.2.2).

REFERENCES

Ábrahám, P., Moór, A., Kiss, Cs., Héraudeau, P., & del Burgo, C. 2003, in Exploiting the *ISO* Data Archive: Infrared Astronomy in the Internet Age, ed. C. Gry et al. (ESA SP-511; Noordwijk: ESA), 129
Ardila, D. R., et al. 2004, ApJ, 617, L147
Artymowicz, P. 1996, in The Role of Dust in the Formation of Stars, ed. H. U. Kaüfl & R. Siebenmorgen (New York: Springer), 137
Aumann, H. H., et al. 1984, ApJ, 278, L23
Backman, D., & Gillett, F. C. 1987, in Cool Stars, Stellar Systems and the Sun, ed. J. L. Linsky & R. E. Stencel (Berlin: Springer), 340
Backman, D. E., & Paresce, F. 1993, in Protostars and Planets III, ed. E. H. Levy & J. I. Lunine (Tucson: Univ. Arizona Press), 1253
Barrado y Navascués, D. 1998, A&A, 339, 831
Barrado y Navascués, D., Stauffer, J. R., Song, I., & Caillault, J.-P. 1999, ApJ, 520, L123
Beichman, C. A., Neugebauer, G., Habing, H. J., Clegg, P. E., & Chester, T. J., eds. 1988, *IRAS* Explanatory Supplement (Washington, DC: GPO)
Beichman, C. A., et al. 2005a, ApJ, 622, 1160
———. 2005b, ApJ, 626, 1061
Binney, J. J., Dehnen, W., Houk, N., Murray, C. A., & Penston, M. J. 1997, in *Hipparcos*, Venice '97, ed. B. Battrick (ESA SP-402; Noordwijk: ESA), 473
Bryden, G., et al. 2006, ApJ, 636, 1098
Carpenter, J. M., Wolf, S., Schreyer, K., Launhardt, R., & Henning, T. 2005, AJ, 129, 1049
Chen, C. H., Jura, M., Gordon, K. D., & Blaylock, M. 2005a, ApJ, 623, 493
Chen, C. H., et al. 2005b, ApJ, 634, 1372
Cutri, R. M., et al. 2003, Explanatory Supplement to the 2MASS All Sky Data Release (Pasadena: IPAC)
Decin, G., Dominik, C., Malfait, K., Mayor, M., & Waelkens, C. 2000, A&A, 357, 533
Decin, G., Dominik, C., Waters, L. B. F. M., & Waelkens, C. 2003, ApJ, 598, 636
de la Reza, R., & Pinzón, G. 2004, AJ, 128, 1812
Dent, W. R. F., Walker, H. J., Holland, W. S., & Greaves, J. S. 2000, MNRAS, 314, 702
de Zeeuw, P. T., Hoogerwerf, R., de Bruijne, J. H. J., Brown, A. G. A., & Blaauw, A. 1999, AJ, 117, 354
Dominik, C., & Decin, G. 2003, ApJ, 598, 626
Eggen, O. J. 1989, PASP, 101, 54
ESA. 1997, The *Hipparcos* and Tycho Catalogues (ESA SP-1200; Noordwijk: ESA)
Evans, D. S. 1967, in IAU Symp. 30, Determination of Radial Velocities and Their Applications, ed. A. H. Batten & J. F. Heard (London: Academic Press), 57
Favata, F., Barbera, M., Micela, G., & Sciortino, S. 1993, A&A, 277, 428
Gabriel, C., Acosta-Pulido, J., Heinrichsen, I., Morris, H., & Tai, W.-M. 1997, in ASP Conf. Ser. 125, Astronomical Data Analysis Software and Systems VI, ed. G. Hunt & H. E. Payne (San Francisco: ASP), 108
Gerbaldi, M., Faraggiana, R., Burnage, R., Delmas, F., Gómez, A. E., & Grenier, S. 1999, A&AS, 137, 273
Girardi, L., Bressan, A., Bertelli, G., & Chiosi, C. 2000, A&AS, 141, 371
Gordon, K. D., et al. 2005, PASP, 117, 503
Greaves, J. S., Mannings, V., & Holland, W. S. 2000, Icarus, 143, 155

Greenberg, J. M. 1998, A&A, 330, 375
Grenier, S., et al. 1999, A&AS, 137, 451
Habing, H. J., et al. 2001, A&A, 365, 545
Harper, D. A., Loewenstein, R. F., & Davidson, J. A. 1984, ApJ, 285, 808
Heinrichsen, I., Walker, H. J., Klaas, U., Sylvester, R. J., & Lemke, D. 1999, MNRAS, 304, 589
Helou, G., & Walker, D. W., eds. 1988, *IRAS* Catalogs: The Small Scale Structure Catalog (Washington, DC: GPO)
Hines, D. C., et al. 2005, FEPS Data Explanatory Supplement, Version 3.0 (Pasadena: SSC)
Holland, W., et al. 1998, Nature, 392, 788
Jarrett, T. H., Chester, T., Cutri, R., Schneider, S., & Huchra, J. P. 2000, AJ, 119, 2498
Jura, M. 1991, ApJ, 383, L79
Jura, M., White, R., Telesco, C., Pina, R., & Fisher, R. S. 1998, ApJ, 505, 897
Jura, M., et al. 2004, ApJS, 154, 453
Kalas, P. 2005, ApJ, 635, L169
Kalas, P., Graham, J. R., Beckwith, S. V. W., Jewitt, D. C., & Lloyd, J. P. 2002, ApJ, 567, 999
Kenyon, S. J. 2002, PASP, 114, 265
Kenyon, S. J., & Bromley, B. C. 2002, ApJ, 577, L35
———. 2004, AJ, 127, 513
Kessler, M. F., et al. 1996, A&A, 315, L27
Kharchenko, N. V., Piskunov, A. E., & Scholz, R.-D. 2004, Astron. Nachr., 325, 439
Kim, J. S, et al. 2005, ApJ, 632, 659
King, J. R., Villarreal, A. R., Soderblom, D. R., Gulliver, A. F., & Adelman, S. J. 2003, AJ, 125, 1980
Kleinmann, S. G., Cutri, R. M., Young, E. T., Low, F. J., & Gillett, F. C. 1986, Explanatory Supplement to the *IRAS* Serendipitous Survey Catalog (Pasadena: JPL)
Koerner, D. W., Ressler, M. E., Werner, M. W., & Backman, D. E. 1998, ApJ, 503, L83
Krist, J. E., et al. 2005, AJ, 129, 1008
Lachaume, R., Dominik, C., Lanz, T., & Habing, H. J. 1999, A&A, 348, 897
Lallement, R., Welsh, B. Y., Vergely, J. L., Crifo, F., & Sfeir, D. 2003, A&A, 411, 447
Laureijs, R. J., Klaas, U., Richards, P. J., Schulz, B., & Ábrahám, P. 2003, The *ISO* Handbook, Vol. 4: PHT—The Imaging Photo-Polarimeter, Version 2.0.1 (ESA SP-1262; Noordwijk: ESA)
Leggett, S. K. 1992, ApJS, 82, 351
Lemke, D., et al. 1996, A&A, 315, L64
Lisse, C., et al. 2002, ApJ, 570, 779
Liu, M. C., Matthews, B. C., Williams, J. P., & Kalas, P. G. 2004, ApJ, 608, 526
Low, F. J., Smith, P. S., Werner, M., Chen, C., Krause, V., Jura, M., & Hines, D. C. 2005, ApJ, 631, 1170
Lowrance, P. J., et al. 2000, ApJ, 541, 390
Luhman, K. L., Stauffer, J. R., & Mamajek, E. E. 2005, ApJ, 628, L69
Magakian, T. Y. 2003, A&A, 399, 141
Makovoz, D., & Marleau, F. 2005, PASP, 117, 1113
Mamajek, E. E. 2004, Ph.D. thesis, Univ. Arizona
Mamajek, E. E., Meyer, M. R., Hinz, P. M., Hoffmann, W. F., Cohen, M., & Hora, J. L. 2004, ApJ, 612, 496
Mamajek, E. E., Meyer, M. R., & Liebert, J. 2002, AJ, 124, 1670
Mannings, V., & Barlow, M. 1998, ApJ, 497, 330
Meyer, M. R., et al. 2004, ApJS, 154, 422
Meynet, G., Mermilliod, J.-C., & Maeder, A. 1993, A&AS, 98, 477
Montes, D., et al. 2001, MNRAS, 328, 45
Moshir, M., et al. 1989, Explanatory Supplement to the *IRAS* Faint Source Survey (Pasadena: JPL)
Nordström, B., et al. 2004, A&A, 418, 989
Oudmaijer, R. D., van der Veen, W. E. C. J., Waters, L. B. F. M., Trams, N. R., Waelkens, C., & Engelsman, E. 1992, A&AS, 96, 625
Patten, B. M., & Willson, L. A. 1991, AJ, 102, 323
Plets, H., & Vynckier, C. 1999, A&A, 343, 496
Rebull, L. M., Stapelfeldt, K. R., Chen, C., Werner, M. W., Song, I., & Zuckerman, B. 2004, BAAS, 205, 17.03
Rieke, G. H., et al. 2004, ApJS, 154, 25
———. 2005, ApJ, 620, 1010
Rocha-Pinto, H. J., Flynn, C., Scalo, J., Hänninen, J., Maciel, W. J., & Hensler, G. 2004, A&A, 423, 517
Sadakane, K., & Nishida, M. 1986, PASP, 98, 685
Sartori, M. J., Lépine, J. R. D., & Dias, W. D. 2003, A&A, 404, 913
Schneider, G., Silverstone, M. D., & Hines, D. C. 2005, ApJ, 629, L117
Schneider, G., et al. 1999, ApJ, 513, L127
Silverstone, M. D. 2000, Ph.D. thesis, UCLA
Skuljan, J., Hearnshaw, J. B., & Cottrell, P. L. 1999, MNRAS, 308, 731
Smith, B., & Terrile, R. 1984, Science, 226, 1421
Song, I., Caillault, J.-P., Barrado y Navascués, D., & Stauffer, J. R. 2001, ApJ, 546, 352
Song, I., Caillault, J.-P., Barrado y Navascués, D., Stauffer, J. R., & Randich, S. 2000, ApJ, 533, L41
Song, I., Zuckerman, B., & Bessell, M. S. 2003, ApJ, 599, 342
———. 2004, ApJ, 614, L125
Spangler, C., Sargent, A. I., Silverstone, M. D., Becklin, E. E., & Zuckerman, B. 2001, ApJ, 555, 932
Stauffer, J. R., Schultz, G., & Kirkpatrick, J. D. 1998, ApJ, 499, L199
Stauffer, J. R., et al. 2005, AJ, 130, 1834
Stelzer, B., & Neuhäuser, R. 2000, A&A, 361, 581
Stencel, R. E., & Backman, D. E. 1991, ApJS, 75, 905
Strassmeier, K., Washuettl, A., Granzer, Th., Scheck, M., & Weber, M. 2000, A&AS, 142, 275
Sylvester, R., & Mannings, V. 2000, MNRAS, 313, 73
Thi, W. F., et al. 2001, ApJ, 561, 1074
Torres, C. A. O., da Silva, L., Quast, G. R., de la Reza, R., & Jilinski, E. 2000, AJ, 120, 1410
Torres, C. A. O., Quast, G. R., de la Reza, R., da Silva, L., & Melo, C. H. F. 2003, in ASP Conf. Ser. 287, Galactic Star Formation across the Stellar Mass Spectrum, ed. J. M. De Buizer & N. S. van der Bliek (San Francisco: ASP), 439
Uzpen, B., et al. 2005, ApJ, 629, 512
Walker, H. J., & Heinrichsen, I. 2000, Icarus, 143, 147
Webb, R. A., Zuckerman, B., Platais, I., Patience, J., White, R. J., Schwartz, M. J., & McCarthy, C. 1999, ApJ, 512, L63
Weintraub, D. A., Saumon, D., Kastner, J. H., & Forveille, T. 2000, ApJ, 530, 867
Werner, M. W., et al. 2004, ApJS, 154, 1
Williams, J. P., Najita, J., Liu, M. C., Bottinelli, S., Carpenter, J. M., Hillenbrand, L. A., Meyer, M. R., & Soderblom, D. R. 2004, ApJ, 604, 414
Wilson, R. E. 1953, General Catalogue of Stellar Radial Velocities (Washington, DC: Carnegie Inst. Washington)
Wright, C. O., Egan, M. P., Kraemer, K. E., & Price, S. D. 2003, AJ, 125, 359
Wright, J. T., Marcy, G. W., Butler, R. P., & Vogt, S. S. 2004, ApJS, 152, 261
Wyatt, M. C. 2005, A&A, 433, 1007
Zuckerman, B. 2001, ARA&A, 39, 549
Zuckerman, B., & Song, I. 2004a, ApJ, 603, 738
———. 2004b, ARA&A, 42, 685
Zuckerman, B., Song, I., Bessel, M. S., & Webb, R. A. 2001a, ApJ, 562, L87
Zuckerman, B., Song, I., & Webb, R. A. 2001b, ApJ, 559, 388
Zuckerman, B., & Webb, R. A. 2000, ApJ, 535, 959